POLITECNICO DI TORINO

Master's Degree in Automotive Engineering

Master's Degree Thesis

Modelling and Control of Alternative Hybrid Propulsion Systems for High Efficiency Heavy-Duty Vehicles, and Hardware-in-the-Loop Considerations

Supervisors

Prof. Angelo BONFITTO

PhD Candidate Saulius PAKŠTYS

Candidate

Arash MORADI ESPELI

July 2024

Summary

The development of hybrid electric propulsion systems offers significant opportunities to enhance vehicle efficiency and reduce greenhouse gas emissions, particularly for heavy-duty vehicles. This thesis explores the integration of advanced energy storage systems, including batteries, supercapacitors, and fuel cells, within electric vehicles. The primary goal is to optimize energy management strategies and then prepare the vehicle model and control strategies for Hardware-in-the-Loop (HIL) testing to validate these systems under realistic conditions.

Initially, the study focuses on a Battery Electric Vehicle (BEV) model using a BYD K9 series bus as the baseline. The simulation environment replicates the vehicle's dynamics and integrates various control strategies. The BEV model serves as a reference to evaluate the benefits of incorporating additional energy sources like supercapacitors and fuel cells.

The hybrid energy storage system (HESS) is introduced to enhance the BEV's performance. By adding a supercapacitor bank alongside the battery, the vehicle's ability to handle high power demands and capture regenerative braking energy improves. This integration reduces battery stress, and extends its lifespan. The thesis examines different configurations and control strategies for the HESS, including rule-based, adaptive rule-based, and fuzzy logic controllers.

Building upon the BEV enhanced with supercapacitors, the next step involves integrating a fuel cell to further optimize the system, resulting in a Fuel Cell Hybrid Electric Vehicle (FCHEV). The objective is to significantly reduce the battery size by leveraging the fuel cell stack as the primary energy source. Moreover, another control strategy was introduced in this phase called the adaptive neuro-fuzzy inference system (ANFIS). The ANFIS controller was used to enhance adaptability to changing vehicle mass and improve overall energy management. It combines the learning capabilities of neural networks with the fuzzy logic control's ability to handle uncertainty, leading to more efficient power distribution and better vehicle performance under varying load conditions.

The simulations show a 25% reduction in battery C-rate for the powertrain configuration that includes both a battery and a supercapacitor bank. Additionally, in the powertrain setup featuring a battery, fuel cell, and supercapacitor bank, the

overall mass of the HESS is reduced by 495 kg (a 15% reduction) compared to the baseline BEV model, while maintaining the vehicle's range.

To validate the simulation results, HIL testing is proposed. This involves integrating hardware components with the simulation models to evaluate system performance under various conditions. One of key components in setting up the test bench for HIL testing is the modular supercapacitor bank. The modular design of the supercapacitor bank, developed and 3D printed as part of this research, allows for flexible testing and optimization of different configurations.

In summary, this thesis contributes to the development of more efficient and environmentally friendly electric vehicles with hybrid energy storage systems. It provides a comprehensive analysis of energy management strategies and prepares the groundwork for experimental validation through HIL testing, ensuring the practical applicability of the proposed solutions in real-world scenarios.

Acknowledgements

I am deeply grateful for the support and guidance that made this thesis possible. First, I would like to thank my supervisors, Professor Angelo Bonfitto, for his invaluable insights and for giving me the opportunity to explore this field further.

A special thanks to PhD candidate Saulius Pakštys. Without his unwavering guidance and patience, I would not have reached this point. His support has been fundamental throughout my journey. I am deeply thankful for all your assistance.

I am immensely thankful to my family—my mother, father, and sister—whose love and energy have always been with me and pushing me forward despite the physical distance between us. I love you all very much.

To my girlfriend, the love of my life, Sogol, your constant presence and encouragement have been my rock. You stood by me during the toughest times, offering support and love when I needed it the most. Thank you for being there and believing in me.

I extend my gratitude to my friends and colleagues, especially Orazio, Gianmarco, Angelo, Ignazio, and Rami. Your friendship and shared experiences have made this journey more bearable.

Table of Contents

List of Tables

List of Figures

Chapter 1

Introduction

1.1 Background and Legislative Context

The growing awareness of climate change and global warming has highlighted the need to adopt sustainable practices across various sectors. One critical area contributing significantly to greenhouse gas (GHG) emissions is the transportation sector, responsible for about a quarter of total CO2 emissions in Europe, with road transport contributing 71.7% of this total [1]. The reliance on fossil fuels for personal and commercial mobility has resulted in numerous negative environmental impacts, propelling climate change forward.

Governments and institutions worldwide are increasingly pushing for developing and marketing environmentally friendly solutions by implementing stringent regulations. For example, initiatives such as the European Union's "Fit for 55" [1] package and the European Green Deal [2] aim to reduce emissions significantly, prompting the automotive industry to invest heavily in research and development of alternatives to traditional internal combustion engines (ICEs).

Considering that a 46.5% share of road transport emissions is emitted by commercial vehicles [3], the research into hybrid propulsion systems for heavy-duty vehicles becomes crucial. The development and optimization of alternative powertrains, particularly for heavy-duty, offer a significant opportunity to reduce overall emissions and improve fuel efficiency. This project aims to address these critical issues by exploring advanced hybrid propulsion systems and preparing the necessary considerations for future Hardware-in-the-Loop (HIL) testing.

1.2 Overview of Hybrid Electric Propulsion Systems

Vehicles can be classified into three groups: internal combustion engine vehicles (ICEV), hybrid electric vehicles (HEV) and all-electric vehicles (AEV). Figure 1.1

shows all available vehicle types.

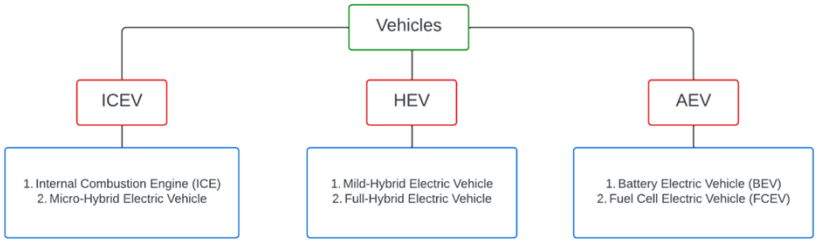

Figure 1.1: The Classification of Vehicles.

1.2.1 Hybrid Electric Vehicles

Hybrid electric vehicles (HEVs) combine an internal combustion engine (ICE) with one or more electric machines (EMs) to create a propulsion system that leverages the strengths of both technologies. This combination allows HEVs to reduce fuel consumption and emissions, particularly in urban driving conditions where stop-and-go traffic is common [4].

HEVs can be classified based on the degree of hybridization, ranging from mild hybrids to full hybrids. Mild hybrids use an electric motor to assist the ICE during acceleration and to recover energy during braking, whereas full hybrids can operate on electric power alone for short distances [5].

The architecture of HEVs can be categorized into series, parallel, and series-parallel configurations.

- In a series hybrid, the ICE drives a generator that produces electricity, which in turn powers the electric motor. This configuration allows the ICE to operate at its most efficient point, but it also requires two energy conversions, leading to efficiency losses. Within the series hybrid classification, there are three sub-classifications of architecture, which depend on the sizes of the ICE, the electric generator, and the battery.
  - Range Extender: In increasing sizes of the ICE and electric generator and in decreasing size of the battery, the architectures are known as Range Extender, where the ICE is used to recharge the battery a little bit in long-range travel.
  - Load Follower: Where the engine sustains the charge of the battery.
  - Full Performance: Which offers the flexibility to increase the efficiency of the engine by choosing its operating points, as shown in Figure 1.2.

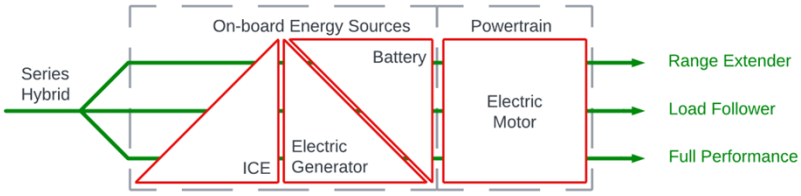

Figure 1.2: Degree of Hybridization for Series HEV.

- In contrast, a parallel hybrid allows both the ICE and the electric motor to drive the vehicle's wheels directly. This reduces the need for energy conversions and can improve overall efficiency, especially during highway driving. However, the control strategies for managing the power split between the ICE and the electric motor can be complex.
- Series-parallel hybrids combine elements of both series and parallel architectures, allowing for greater flexibility in optimizing the vehicle's performance. These systems can switch between series and parallel modes depending on the driving conditions, offering a balance between efficiency and complexity.

1.2.2 Battery Electric Vehicle

Battery Electric Vehicles (BEVs) are powered entirely by electric energy stored in batteries, distinguishing them from hybrid vehicles which combine internal combustion engines with electric propulsion systems. BEVs use electric motors to drive the vehicle, eliminating the need for an internal combustion engine and, consequently, the emissions associated with fuel combustion. This characteristic makes BEVs a critical component in reducing greenhouse gas emissions and combating climate change [6], [7].

BEVs offer several advantages over traditional internal combustion engine (ICE) vehicles. One of the primary benefits is the zero tailpipe emissions, which significantly reduce urban air pollution and contribute to improved public health. Additionally, BEVs tend to have fewer moving parts than ICE vehicles, resulting in lower maintenance costs and greater reliability.

The efficiency of BEVs is another notable advantage. BEVs convert over 77% of the electrical energy from the grid to power at the wheels, compared to conventional gasoline vehicles, which convert only about 12%-30% of the energy stored in gasoline to power at the wheels. This higher efficiency translates to lower operating costs for BEV owners, as electricity is generally cheaper than gasoline on a per-mile basis [6], [7].

However, BEVs also face several challenges. One of the most significant is the limited driving range. This limitation is often referred to as "range anxiety" and is a critical factor for consumers when considering a BEV. Moreover, the power request

for a heavy vehicle is higher than for a lighter one, so the battery will be subjected to higher C-rates, or currents, which result in a faster decrease of battery life [8].

Charging infrastructure and time are additional challenges. Fully charging a BEV can take anywhere from 30 minutes to several hours, depending on the charging station and battery capacity. The availability of fast-charging stations is increasing, but it remains a barrier to widespread BEV adoption, particularly in regions with less developed infrastructure.

The batteries themselves are a critical component of BEVs, and advancements in battery technology are continuously improving their performance, lifespan, and safety. Current BEVs primarily use lithium-ion batteries, known for their high energy density and efficiency. However, researchers are exploring alternative battery technologies, such as solid-state batteries, which promise even greater energy densities and faster charging times.

Therefore, while BEVs present a promising solution to reduce greenhouse gas emissions and dependence on fossil fuels, their widespread adoption hinges on overcoming challenges related to driving range, charging infrastructure, and battery technology. Continued research and development in these areas are essential to make BEVs a more viable option for consumers and to realize their full environmental benefits.

1.2.3 Fuel Cell Hybrid Electric Vehicle

Fuel cell electric vehicles (FCEVs) rely solely on fuel cells to power the transmission system, lacking any auxiliary energy source. As a result, fully FCEVs are incapable of energy recovery and require an additional energy source to enable regenerative capabilities. This is where Fuel Cell Hybrid Electric Vehicles (FCHEVs) come into play, integrating a secondary energy source to enable energy recovery capabilities.

The FCHEV is classified as a hybrid vehicle because it utilizes at least two power sources: the fuel cell stack and the battery. Additionally, a supercapacitor cell stack can be included. According to the Beretta method [9], it is technically a series hybrid vehicle since it only has one mechanical actuator, the electric machine. However, to avoid confusion when distinguishing between different powertrain architectures at the power source level, the Beretta method terms will not be applied here. This thesis examines the powertrain architectures for the FCHEV, referred to as "parallel" and "series," based on the positioning of the fuel cell stack relative to the battery.

FCHEVs combine fuel cells with other energy storage systems, such as batteries and ultracapacitors in a series architecture, to address the limitations of using a single energy source. This hybridization helps overcome the slow dynamic response of fuel cells and enhances the overall efficiency and performance of the vehicle and making it a appropriate use case for heavy commercial vehicles. FCHEVs are recognized for their high energy efficiency, environmental benefits, and long driving range, making them a promising solution for sustainable transportation [10]. To be more specific, this solution solves one major issue of regular HEVs which is CO2 emissions during

the Tank-To-Wheel phase and their dependence on fossil fuels [11].

Fuel cells, particularly proton exchange membrane fuel cells (PEMFCs), use hydrogen to generate electricity through a chemical reaction, producing only water and heat as by-products. This process allows FCHEVs to operate with zero tailpipe emissions, contributing significantly to reducing air pollution and greenhouse gas emissions. However, fuel cells alone are not well-suited for the rapid power demands of acceleration and sudden load changes, which can affect their durability and efficiency. To mitigate these issues, FCHEVs incorporate batteries or ultracapacitors to provide additional power during high-demand situations and to recover energy during braking [12]. There are three primary configurations for FCHEVs:

- Fuel Cell-Battery Hybrid: This setup uses a battery to complement the fuel cell, providing power during peak demand and storing energy during periods of low demand.
- Fuel Cell-Ultracapacitor Hybrid: Ultracapacitors, known for their fast dynamic response and high power density, support the fuel cell during rapid power changes.
- Fuel Cell-Battery-Ultracapacitor Hybrid: This configuration combines the benefits of both batteries and ultracapacitors, offering a balanced solution for energy storage and power management [12].

Effective energy management systems (EMS) are crucial for optimizing the performance of FCHEVs. These systems manage the power distribution between the fuel cell and the auxiliary energy sources to minimize hydrogen consumption, extend the fuel cell's lifespan, and enhance the overall efficiency of the vehicle.

1.2.4 Supercapacitors in Hydrid Electric Vehicles

Supercapacitors, also known as ultracapacitors or electrochemical capacitors, are energy storage devices that offer high power density, rapid charge and discharge capabilities, and long cycle life, making them highly suitable for use in hybrid electric vehicles (HEVs). Unlike traditional batteries, supercapacitors store energy electrostatically rather than chemically, which enables them to deliver quick bursts of energy and efficiently capture regenerative braking energy [13].

One of the main advantages of supercapacitors in HEVs is their ability to complement batteries by providing high power for acceleration and capturing energy during braking. This hybrid energy storage system (HESS) improves overall vehicle efficiency, extends battery life, and enhances performance under dynamic driving conditions. Supercapacitors have low internal resistance, which allows for high efficiency and fast energy transfer, making them ideal for applications requiring frequent and rapid energy fluctuations. Therefore, they can be added in parallel to the batteries as an additional power source for the electric machine and reduce the high C-rates experienced by batteries.

The development of advanced materials and manufacturing techniques has further enhanced the performance and application of supercapacitors in HEVs. Researchers have explored various electrode materials, such as carbon-based materials, metal oxides, and conducting polymers, to improve the energy storage capacity and durability of supercapacitors. Additionally, new hybridization strategies and energy management systems (EMS) have been developed to optimize the interaction between supercapacitors and other energy storage components in HEVs [13].

1.2.5 Power Converter Configurations and Energy Sources Architectures

Power converters are crucial components in hybrid electric vehicles (HEVs), responsible for managing the conversion and distribution of electrical energy between the vehicle's various subsystems. These converters can be classified into three primary categories: AC-DC converters, DC-DC converters, and DC-AC converters, each serving specific roles within the vehicle's powertrain [14].

- AC-DC Converters: These converters are used primarily for charging the vehicle's battery from an external AC power source. The Vienna rectifier is a notable AC-DC converter that offers high efficiency and compact design, making it suitable for onboard and offboard charging systems. This rectifier type reduces power losses and improves reliability, crucial for efficient battery charging.
- DC-AC Converters (Inverters): These converters are responsible for transforming the DC power from the battery into AC power to drive the electric motor. Multilevel inverters, such as the third harmonic injected seven-level inverter, are highly efficient and reduce the need for intermediate DC-DC converters. These inverters enhance the overall efficiency of the powertrain and support smooth and responsive motor control.
- DC-DC Converters: These converters manage the voltage levels between the battery and other components of the vehicle, such as the electric motor and auxiliary systems. Multi-device interleaved DC-DC boost converters are preferred in HEVs due to their ability to provide high power density and efficient energy conversion. These converters ensure that the electric motor receives the appropriate voltage, optimizing performance and extending the battery's lifespan.

To optimize the use of DC-DC converters in simulations, a look-up table based on the efficiency map of the DC-DC converter was employed [15]. This approach captures how the efficiency of the converter varies with changes in voltage and power, providing a more accurate representation of its performance. By using this method, the study avoids relying on a constant efficiency value, thereby reflecting the real-world behavior of the converter more closely. The choice was made not to

model the physical representation of DC-DC converters, focusing instead on the modeling and control strategies to enhance overall vehicle performance.

For hybrid energy storage system applications containing a battery and supercapacitors, three main types of configurations are used as shown in Figure 1.3: passive, semi-active and fully active [16].

- Topology 1 - Passive: In this configuration, the supercapacitors and the battery are directly connected in parallel with one another, and a DC/DC converter can be added before the DC bus. The main advantage of this configuration is that it is cheap, having few components. However, this results in the impossibility of implementing control strategies at the converter level and the supercapacitors performance is inherently limited.

- Topology 2 - semi-active: In this configuration, the supercapacitors and the battery are separated from each other by a bidirectional DC/DC converter. As for the passive configuration, another DC/DC converter can be added before the DC bus. This configuration allows more flexibility positioning the components. The most commonly used configuration is having the battery directly connected to the DC bus, with no power converter, and the supercapacitors connected to the battery in parallel, separated by a DC/DC converter. It represents a good compromise between control, cost and efficiency but is unable to provide an optimal solution for any of these aspects.

- Topology 3 - Active: in this configuration, in which two bidirectional DC/DC converters, one for the battery and one for the supercapacitors, are used, offers the best control possibilities. However, said control is very complex and the configuration is expensive due to its elevated number of components [16], [17].

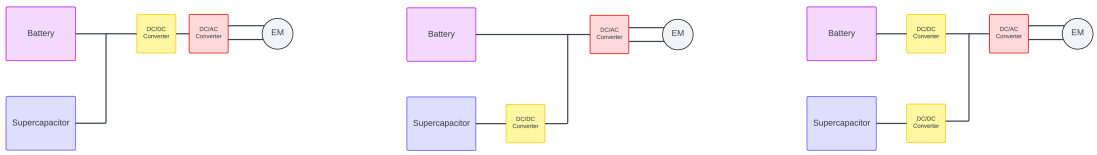

(a) **(b)** **(c)**

Figure 1.3: Hybrid Energy Storage Systems Containing Battery and Supercapacitor Configuration.

When integrating a fuel cell into the system along with the battery and supercapacitors, several configuration options arise as depicted in Figure 1.4:

- Topology 4: This configuration includes both a battery and a supercapacitor as storage. The advantage of this topology is the combination of the power handling capabilities of the supercapacitor with the energy storage capabilities

of the battery. This configuration can also be found with the battery and supercapacitor interchanged.

- Topology 5: This topology comprises a fuel cell stack, battery, and supercapacitor, with DC/DC converters included between all components and the DC bus. Similar to Topology 5, it combines the power handling capabilities of the supercapacitor with the energy storage capabilities of the battery. Additionally, it enables voltage control of the DC bus, albeit with increased complexity [18].

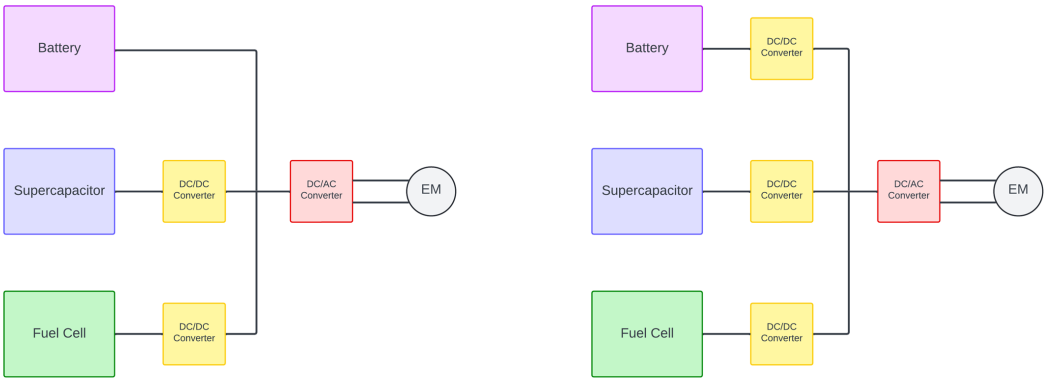

(a) Caption for Image 1 **(b)** Caption for Image 2

Figure 1.4: Hybrid Energy Storage Systems Containing Battery, Supercapacitor and Fuel Cell Configuration.

1.3 Energy Management Strategies

Energy management strategies (EMS) are crucial in hybrid electric vehicles to optimize the use of multiple power sources, enhance efficiency, and extend the lifespan of components. EMS ensure that power is distributed between the batteries, supercapacitors, fuel cells and other energy sources in the most efficient manner. This optimization is essential for reducing fuel consumption, minimizing emissions, and improving overall vehicle performance [19]. There are two levels at which energy management strategies can be considered for hybrid electric vehicles: the powertrain level, where the torque distribution of two or more mechanical actuators is chosen based on their efficiency at a given operating point, and the power source level, where the power distribution between the battery and supercapacitors, for example, is dictated based on SOC concerns and the power demand. Since the fuel cell hybrid architecture, which has only one mechanical actuator, has been chosen for this thesis, the EMS acting at the powertrain level will not be reviewed. EMS can be

broadly categorized into rule-based, adaptive rule-based, fuzzy logic, and adaptive neuro-fuzzy inference system (ANFIS) strategies. These methods provide different levels of control complexity and optimization capabilities, each with its own set of benefits and applications [20]. The rule-based, adaptive rule-based, and fuzzy logic controllers lie within the rule-based control strategies, while the adaptive neuro-fuzzy inference system lies within the global optimization control strategies as can be seen in Figure 1.5.

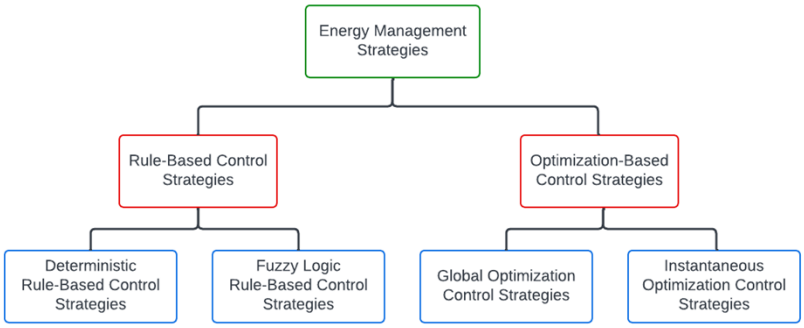

Figure 1.5: Energy Management Strategies.

1.3.1 Rule-Based Control

Rule-based control strategies are the simplest form of EMS. They use predefined rules to manage the power flow between different energy sources based on current operating conditions. These rules are typically derived from heuristics or expert knowledge and are easy to implement. However, they may not always provide optimal performance under all driving conditions. Rule-based control is effective for its simplicity and reliability but can be limited in dynamic and highly variable environments. An example of its use is by the authors of [21], who use the strategy to specify the power distribution between a battery and supercapacitors.

1.3.2 Adaptive Rule-Based Control

Adaptive rule-based control strategies build on the basic rule-based approach by incorporating real-time data and feedback to adjust the control rules dynamically. This adaptability allows the system to better respond to changing driving conditions and optimize performance more effectively than static rule-based systems. Adaptive rule-based control can improve fuel efficiency and reduce emissions by continuously fine-tuning the energy management rules based on real-time information.

1.3.3 Fuzzy Logic Control

Fuzzy logic control strategies use fuzzy logic principles to handle the uncertainty and variability in HEV operations. These strategies translate linguistic control rules into mathematical models that can manage the power flow more flexibly. Fuzzy logic control is particularly useful in complex and non-linear systems where traditional control methods may fall short. It offers a robust and flexible approach to EMS, capable of dealing with imprecise inputs and providing smooth control actions [22].

Structure of Fuzzy Logic Control

Unlike conventional controllers, which have fixed parameters and structure, making their tuning process laborious and intricate, the Fuzzy Logic Controller (FLC) excels in handling systems where exact values for process flow are undefined. Fuzzy logic operates on the principle of "processing linguistic variables instead of precise numbers" and "utilizing descriptive sentences rather than mathematical equations."

The FLC comprises three fundamental processes, illustrated in Figure 1.6. The initial process, fuzzification, transforms input data into crisp values or linguistic variables. There are three primary types of fuzzifiers employed in this stage:

- Gaussian Fuzzifier
- Singleton Fuzzifier
- Triangular/Trapezoidal Fuzzifier

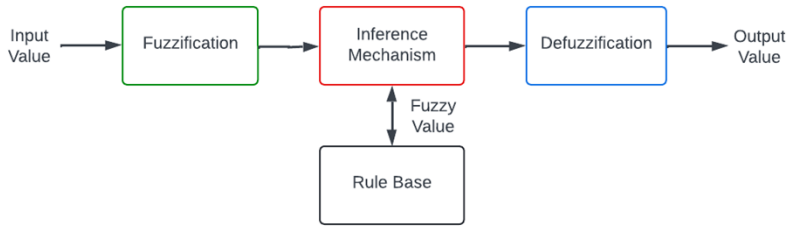

Figure 1.6: Fuzzy Logic Controller Procedure.

The proposed fuzzifier employs triangular shapes for all inputs. These crisp values or fuzzy sets are then used to create rules in the inference-making block, which mimics human decision-making. The two primary types of fuzzy inference systems (FIS) are Mamdani FIS and Takagi–Sugeno–Kang FIS. The final stage, defuzzification, translates linguistic variables back into numerical values or crisp outputs. There are several methods for defuzzification. For the proposed FLC, the center of gravity (COG) method is used, as specified in the following equation:

$$U_{\mathrm{COG}} = \sum_{j=1}^{n} u_c(x_j) x_j \tag{1.1}$$

The term U_{COG} represents the center of gravity, x_{j} denotes a specific point within the universe of discourse, and $u_c(x_j)$ is the membership value of the resulting conclusion [22].

In this thesis, the Sugeno fuzzy inference system was chosen over the Mamdani inference system. Both methods share several similarities: the initial steps of fuzzifying inputs and applying the fuzzy operator are consistent between Mamdani and Sugeno systems. The key difference, however, lies in the output membership functions; Sugeno employs linear or constant functions.
Although the Mamdani system is often considered more intuitive and is widely used, Sugeno was selected for its more compact and computationally efficient nature. Furthermore, Sugeno's compatibility with linear techniques, such as PID control, makes it particularly advantageous for this application [23]. Using the provided inputs, the FLC will create the membership functions. Further details on the ranges for these inputs are explained in the following sections.

1.3.4 Adaptive Neuro-Fuzzy Inference System

The Adaptive Neuro-Fuzzy Inference System (ANFIS) combines the benefits of fuzzy logic and neural networks to create a highly adaptive and intelligent control system. This approach uses neural networks to learn and adapt the fuzzy inference system rules based on historical and real-time data. ANFIS can provide optimal control by continuously improving its performance through learning. This method is highly effective in managing the complex interactions between different energy sources in HEVs, leading to significant improvements in efficiency and performance [19].

ANFIS effectively combines the adaptive learning strengths of neural networks with the logical framework of fuzzy logic. This integration allows ANFIS to model and control complex, nonlinear systems with a high degree of accuracy. By using a hybrid learning algorithm that combines gradient descent and least squares estimation, ANFIS fine-tunes the parameters of the fuzzy inference system, which helps to represent intricate behaviors accurately [24].

ANFIS leverages the learning capabilities of neural networks alongside the decision-making process inherent in fuzzy logic. This fusion is especially beneficial in handling systems with significant uncertainty and imprecision, making it ideal for practical, real-world applications. The hybrid learning process involves backpropagation, which adjusts the membership functions, and a least squares method for optimizing the consequent parameters. This combination enhances the system's precision and efficiency, allowing for a more accurate representation of complex systems [24], [25].

ANFIS is structured to effectively manage complex and dynamic systems, a critical feature for optimizing energy management in hybrid electric vehicles. The structure of ANFIS can be divided into five distinct layers, each playing a crucial role in processing input data and generating precise outputs, as shown in Figure 1.7.

The first layer, known as the Input Layer or Fuzzification Layer, corresponds to the input variables. In this layer, membership functions are applied to transform

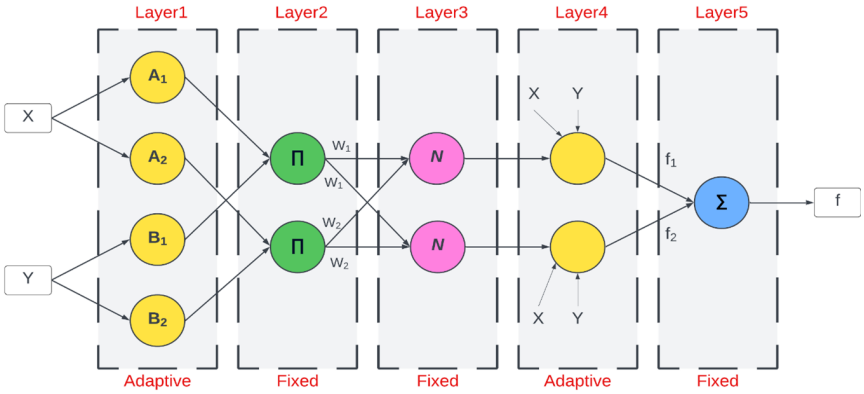

Figure 1.7: Adaptive Neuro-Fuzzy Inference System Procedure.

crisp input values into fuzzy values. This transformation is essential as it allows the system to handle imprecise and uncertain data, setting the foundation for the fuzzy inference process.
The second layer, called the Rule Layer, represents the fuzzy rules. Each node in this layer combines the membership values from the input layer to compute the strength or firing strength of each rule. This computation indicates how well the input data matches the conditions specified by each rule, forming the basis for subsequent processing.
In the third layer, known as the Normalization Layer, the nodes normalize the firing strengths of the rules. This normalization process ensures that the combined rule strengths sum to one, which balances the influence of each rule on the final output. This step is crucial for maintaining the integrity of the inference process.
The fourth layer, referred to as the Defuzzification Layer, is where the outputs of the rules are computed. Typically, these outputs are linear functions of the input variables. This layer translates the fuzzy conclusions derived from the rule layer back into crisp values, making them usable for practical decision-making.
Finally, the fifth layer, or Output Layer, aggregates the outputs from all the rules to produce the final output. This aggregation process combines the defuzzified values from the previous layer, resulting in a single output value that can be used for decision-making or control purposes in the energy management system.

1.4 Simulation Environment: MATLAB/Simulink Overview

The simulation environment for modeling hybrid electric vehicles (HEVs) and fuel cell hybrid electric vehicles (FCHEVs) is crucial for developing and testing various

control strategies and vehicle configurations. MATLAB/Simulink is widely used for this purpose due to its robust capabilities in handling complex system simulations, providing a flexible platform for integrating different models and control algorithms. This environment allows for the simulation of vehicle dynamics, powertrain components, and energy management systems, facilitating a comprehensive analysis of vehicle performance under various driving conditions.
One of the key features of Simulink is its ability to handle multi-domain simulations. This is particularly important for HEVs and FCHEVs, which involve electrical, mechanical, and thermal domains. Simulink supports the integration of these domains, allowing for the simulation of interactions between electrical components like batteries and supercapacitors, mechanical components like transmissions and drivetrains, and thermal management systems.
Another significant advantage of using MATLAB/Simulink for vehicle modeling is its support for real-time testing and validation. Simulink models can be deployed to hardware-in-the-loop (HIL) systems, enabling the testing of control algorithms and vehicle systems in real-time with actual hardware components. This capability is essential for verifying the performance and robustness of control strategies before implementation in actual vehicles [14].

1.5 Objectives of the Research

The research on hybrid electric propulsion systems aims to address critical challenges in the automotive industry by developing innovative solutions to enhance vehicle efficiency and reduce environmental impact. The specific objectives of this research are:

1. **Optimization of Powertrain Architectures:** Develop and evaluate hybrid powertrain configurations that maximize energy efficiency and minimize emissions. This includes integrating advanced components such as supercapacitors and fuel cells to enhance the performance of the heavy-duty vehicle. This integration is expected to prolong battery life and improve the overall durability of the energy storage system.

2. **Development of Advanced Energy Management Strategies (EMS):** Design and implement various EMS, including rule-based, adaptive rule-based, fuzzy logic, and adaptive neuro-fuzzy inference system (ANFIS) controls. These strategies aim to optimize energy flow within the vehicle, balancing the demands between different power sources to improve overall efficiency and reduce emissions.

3. **Experimental Validation Preparation:** Prepare all necessary steps and considerations for the experimental validation of the developed control strategies using Hardware-in-the-Loop (HIL) setups. This preparation is crucial for

verifying the real-world applicability and performance of the proposed solutions, ensuring they can be effectively implemented in actual vehicle systems. Moreover, a modular supercapacitor bank was designed and 3D printed, to facilitate flexible testing and optimization of different configurations. The modular design allows for easy reconfiguration and testing of various control strategies and load conditions in the HIL setup.

By achieving these objectives, the research aims to contribute to the development of more sustainable and efficient transportation solutions, supporting global efforts to reduce greenhouse gas emissions and combat climate change.

Chapter 2

Battery - Supercapacitor Hybrid Electric Storage System

2.1 Baseline Vehicle Modeling

The studied BEV vehicle is the BYD K9 series 12-meter-long eBUS [15-not in zotero], which is taken to be the baseline vehicle. Tables 2.1 and 2.2 outline its main characteristics.

Dimension/Weight			
Parameter	**Notation**	**Unit**	**Value**
Length/Width/Height	L/W/H	m	12.05/2.55/3.36
Mass	M	kg	13000
Gross Curb Weight	GCW	kg	16000
Wheelbase	L	m	5.9
Height of CG	h_G	m	0.5
Frontal area	A_f	m^2	8.568
Drag coefficient	C_d	-	0.5
Tire inertia	I_t	$kg{\cdot}m^2$	0.8
Rolling radius	r	m	0.49

Table 2.1: Vehicle Dimension and Weight Characteristics

The vehicle model examined in this thesis utilizes a forward modeling approach, as illustrated in Figure 2.1. This forward architecture was selected over a backward architecture because it is more suitable for component evaluation. In a forward architecture, the model predicts future states based on the current state and control

Powertrain			
Parameter	**Notation**	**Unit**	**Value**
Maximum Power	$P_{\max}$	kW	300 (2x150)
Maximum Torque	$T_{\max}$	Nm	1100 (2x550)
Battery (Lithium-Iron Phosphate LFP)			
Parameter	**Notation**	**Unit**	**Value**
Rated Operational Voltage	V	V	540
Energy	E	kWh	324
Capacity	C	Ah	600

Table 2.2: Vehicle Powertrain and Battery Characteristics

inputs, whereas a backward architecture determines the control inputs needed to achieve a desired future state from the current state. Additionally, the forward architecture provides results that are more reflective of real-world scenarios since it facilitates the incorporation of a driver model acting as the actuator.

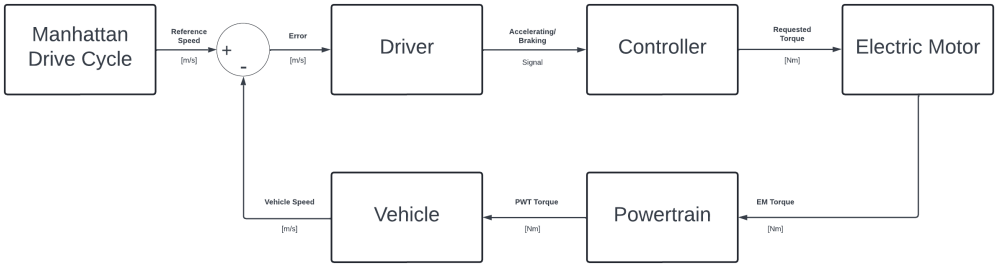

Figure 2.1: Forward Vehicle Model Structure.

In Simulink, the model is structured into two primary components: the controller and the plant. The inputs and outputs of these components are depicted in Figure 2.2.

The controller, depicted in Figure 2.3, generates the speed profile using the loaded drive cycle as a reference. It calculates the error as the difference between the reference speed and the current speed of the vehicle. This error is processed by a Proportional-Integral (PI) controller, which converts it into a normalized signal for acceleration or braking. The output from the PI controller is then translated into a signal indicating the required torque for the Electric Machine (EM). This torque signal is compared with the EM's limit at the current operating point and, if necessary, is saturated before being sent to the plant, along with the brake signal.

To generate the driving cycle, real speed and position data collected from a bus operating on the streets of Manhattan were utilized. This driving cycle, which features frequent stops, has been employed in the literature for the homologation of city buses [26]. The characteristics of the driving cycle are summarized in Table 2.3.

The plant, depicted in Figure 2.4, includes a model of the vehicle's longitudinal

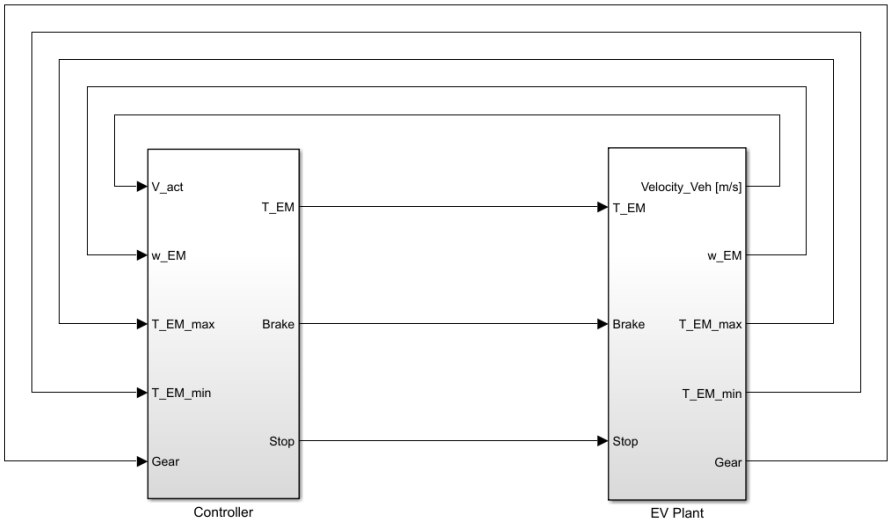

Figure 2.2: General Structure of Simulink Model.

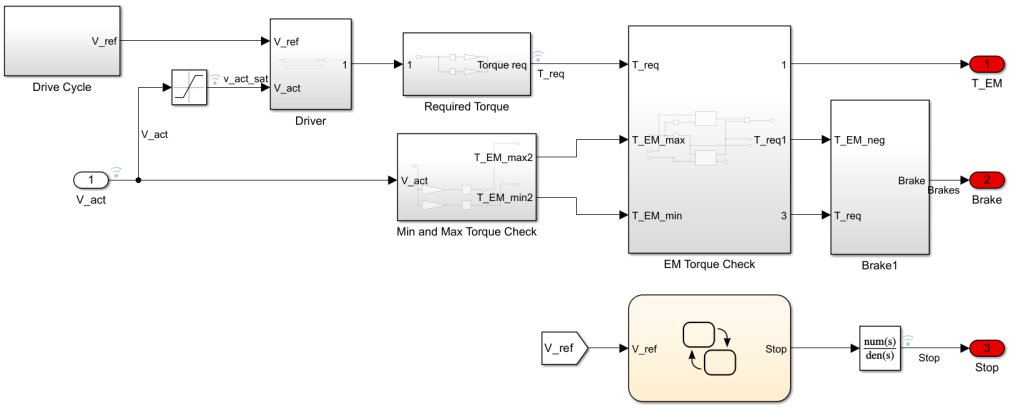

Figure 2.3: Controller Structure of Simulink Model.

Parameter	**Unit**	**Value**
Total Cycle Time	s	1089
Maximum Speed	m/s	11.24
Average Speed	m/s	3.3
Maximum Acceleration	m/s^2	2.04
Covered Distance	km	3.3

Table 2.3: Manhattan Drive Cycle Characteristics

dynamics, which calculates the vehicle's actual speed, tire forces, and horizontal motion. These outputs are then used in the tire modeling also included within the plant. Additionally, the plant encompasses models for the Electric Machine (EM)

and the power sources.

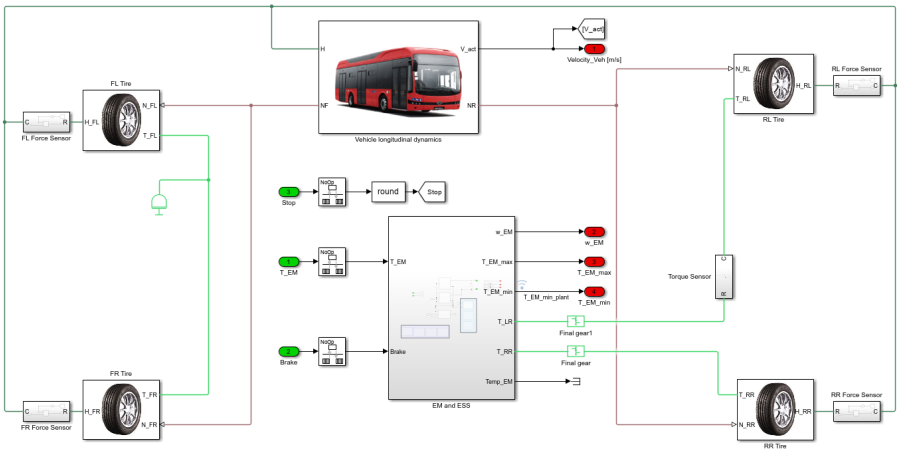

Figure 2.4: Plant Structure of Simulink Model.

The vehicle is equipped with two identical Electric Machines (EMs), each modeled using a look-up table derived from the torque-speed map of an electric motor. This map has been appropriately adjusted using scaling factors to match the characteristics of the electric machines installed in the BYD bus. Figure 2.5 displays the scaled Torque-Speed map. The fourth quadrant of this map, being a mirror image of the first, has been omitted for clarity. The Electric Machine (EM) model generates a power request based on this map, which is subsequently fulfilled by the available power sources. Detailed descriptions of this process will be provided later.

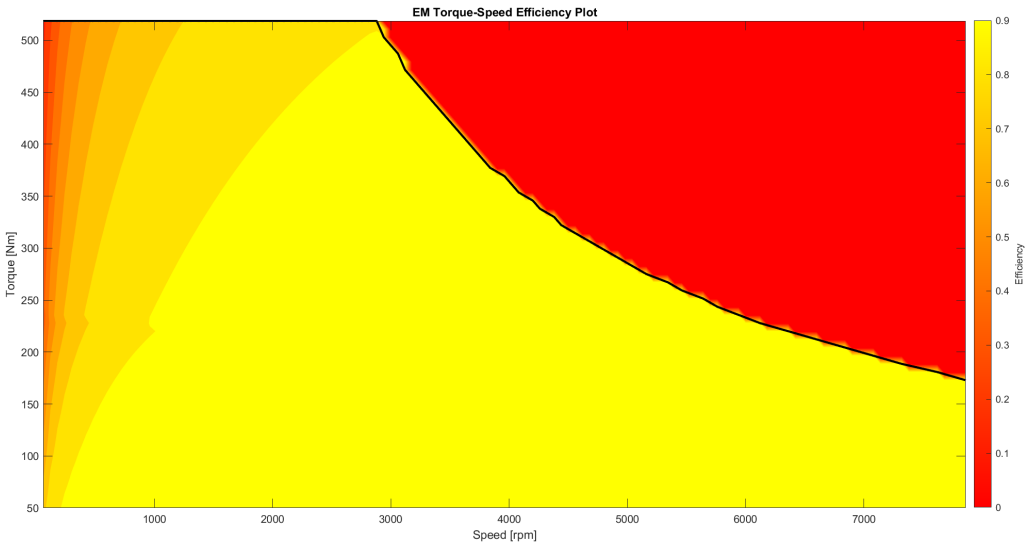

Figure 2.5: Torque-Speed Map of the Electric Machine.

2.2 Battery Electric Vehicle with Supercapacitor Pack Modelling

2.2.1 Hybrid Energy Storage System Architecture

The integration of a supercapacitor pack alongside the battery as a power source necessitates an evaluation of potential configurations to determine the most advantageous setup. As discussed in the introduction, various configurations in which the battery and supercapacitor operate in parallel differ in the relative positioning of the two energy sources and the inclusion of one or more DC/DC converters. For this thesis, the semi-passive configuration (topology 2) has been selected. This involves placing a bidirectional DC/DC converter between the supercapacitor pack and the battery, allowing the voltage to vary and thus maximizing the utilization of the supercapacitor. However, this setup incurs disadvantages such as higher costs, additional system mass, and power losses. A schematic of this configuration is shown in Figure 2.6.

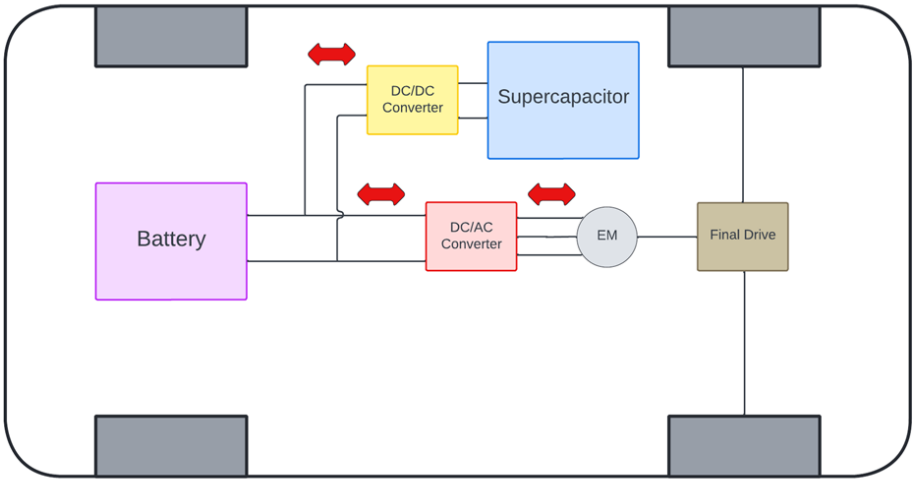

Figure 2.6: Hybrid Energy Storage System Semi-Passive Configuration.

In this work, the decision was made to avoid modeling DC/DC converter components, as the primary focus is to explore control strategies for energy management and analyze its impact rather than the physical representation of individual components. To account for the efficiency drop in DC/DC converters, this study incorporates efficiency variations between different energy sources in the model. Instead of using a constant gain value, a look-up table is employed to consider the efficiency of the DC/DC converter at different voltage levels of the supercapacitor and fuel cell, as indicated in Figure 2.7. This approach allows for a more accurate representation of the DC/DC converter's performance under varying conditions. The efficiency

map data for the DC/DC converter was sourced from the [15] paper. This map was then carefully adjusted with scaling factors to align with the power and voltage specifications of the current system.

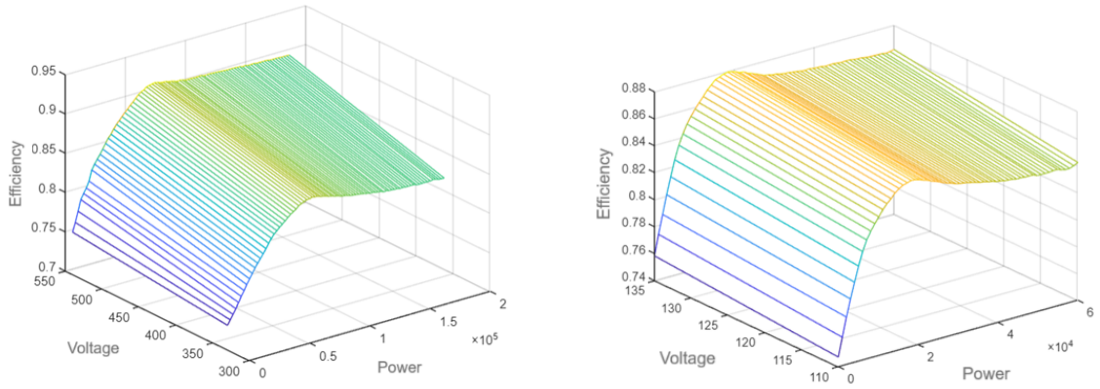

(a) For Supercapacitor **(b)** For Fuel Cell

Figure 2.7: DC/DC Converter Efficiency Map.

2.2.2 Hybrid Energy Storage System Modelling

In this section, the focus will be on the models of the energy sources, specifically the battery and supercapacitor, as depicted in Figure 2.8.

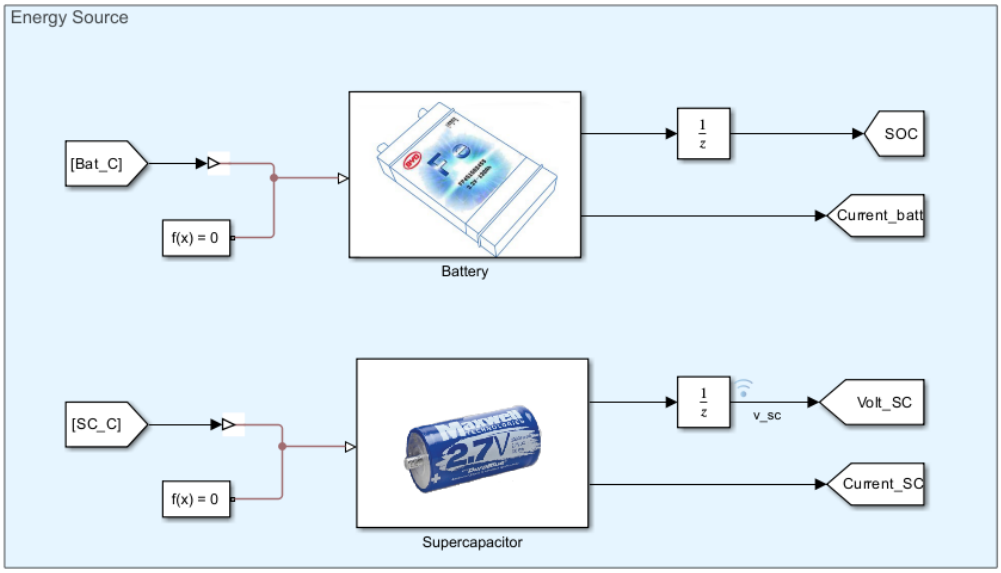

Figure 2.8: Energy Sources Structure in Simulink.

Battery

The main characteristics of the battery used in the BYD electric bus model K9-12 meters are detailed in Table 2.4. The entire battery pack consists of numerous cells arranged in series and parallel to meet the required capacity and voltage. A specific cell manufactured by BYD for the automotive industry, the BCT 200Ah, was selected to adequately fulfill the vehicle's capacity and voltage requirements. The characteristics of this cell are provided in the table below. The battery modules and packs use proprietary LFP chemistry, which offers high energy density. The design of these batteries is illustrated in Figure 2.9.

Parameter	**Unit**	**Value**
Chemistry	-	Lithium-Iron Phosphate
Type of cell	-	Prismatic
Rated Capacity	Ah	200
Rated Voltage	V	3.2
Cell Weight	kg	6.15
Size	mm	390x140x60
Working Temperature	°C	20–60
Cycle Life	-	2000 discharge cycles (< 1C)

Table 2.4: Battery Cell Characteristics

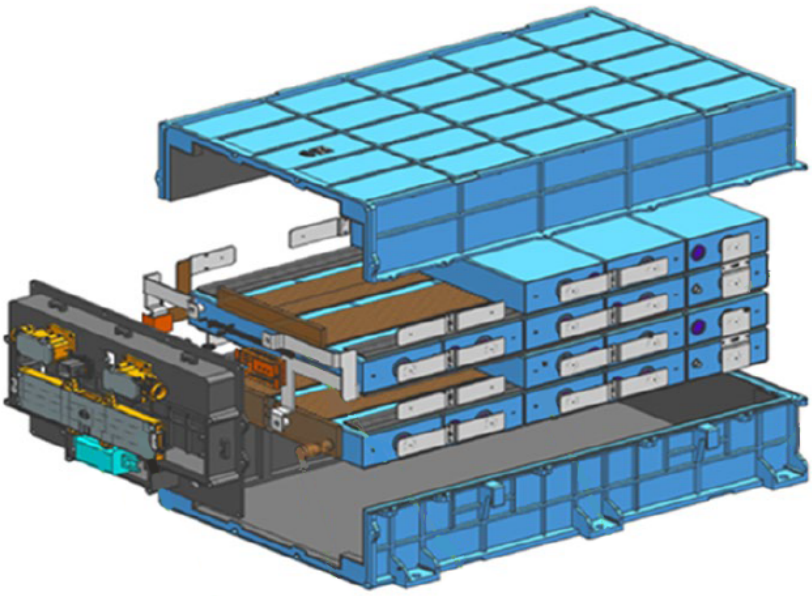

Figure 2.9: BYD Battery Cell Module.

The required number of cells to be connected in series and parallel to form the battery pack is determined through straightforward calculations based on the specifications provided in the vehicle's datasheet. For the series configuration, the total voltage is divided by the voltage of a single cell, while for the parallel configuration, the total battery capacity is divided by the capacity of a single cell. This results in a configuration of 169 cells in series and 3 cells in parallel. The overall mass of the battery can then be calculated, amounting to 3118 kg. In the model, the battery is represented as an ideal voltage source. Its Simulink representation, which has been obtained from prior research conducted at the DIMEAS (Dipartimento Ingegneria Meccanica e Aerospaziale) of Politecnico di Torino, was not developed within the scope of this thesis. Figure 2.10 illustrates how the battery is represented in Simulink.

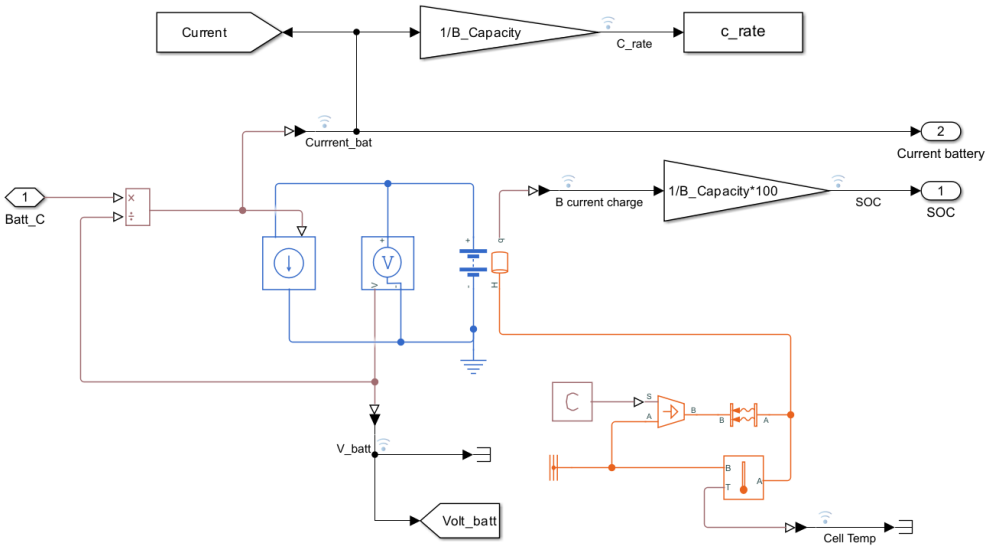

Figure 2.10: Battery Model in Simulink.

Supercapacitor

For the supercapacitor pack, the BCAP3000 P270 K04/05 supercapacitor cell manufactured by Maxwell was selected. Its specifications are detailed in Table 2.5.

The mentioned supercapacitor cell from Maxwell was selected due to its high-power capabilities and common usage in the heavy transport sector. The goal was to match the voltage of the supercapacitor (SC) pack to that of the battery, which is 540 V. To achieve this, 200 cells were connected in series, with only one row of cells in parallel, resulting in a total SC pack mass of 95 kg. The supercapacitor is modeled using various equivalent circuit models. These models incorporate fundamental electrical components like resistors and capacitors, which can be configured as single units or multiple units in series or parallel. Common models include the Stern-Tafel model

Parameter	Unit	Value
Rated Capacitance	F	3000
Max. Rated Capacitance	F	3600
Rated voltage	V	2.7
Peak Current	A	2300
Continuous Current	A	280
Weight	kg	0.475

Table 2.5: Supercapacitor Cell Characteristics

[27], the Zubieta model [28], and the series model [29]. For this work, the Zubieta model was chosen due to its high accuracy and simplicity. The Zubieta model used in this thesis consists of a circuit with three parallel RC time constants featuring fixed resistances and capacitances, as illustrated in Figure 2.11.

In the Zubieta model, the first branch, comprising R0C0 and the voltage-dependent kcvc, represents the response in seconds. The second branch, R1C1, addresses the response in the minute range, while the third branch, R2C2, characterizes the response for durations exceeding several minutes. Additionally, a resistor Rlk is included to simulate the leakage resistance.

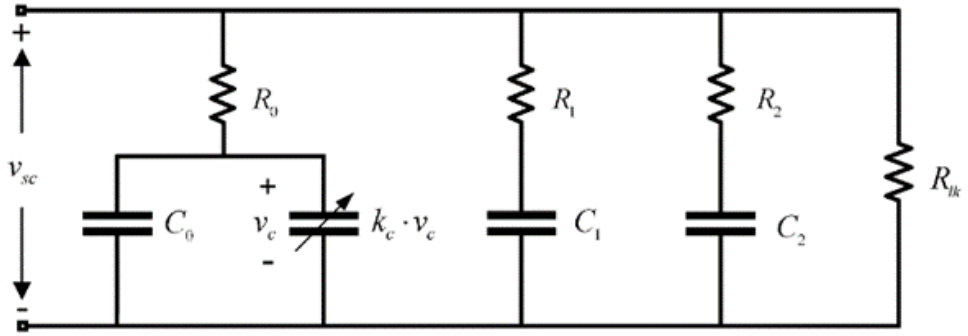

Figure 2.11: Zubieta Model of Supercapacitor Cell.

The characteristics of the selected supercapacitor cell have been determined through experiments conducted by [30] and have been incorporated into this study. These characteristics are detailed in Table 2.6.

The model implemented in Simulink is illustrated in Figure 2.12.

2.3 Control Strategies for Energy Management

As mentioned before, the first part of the manuscript focuses on incorporating a supercapacitor alongside the battery as an additional power source. This involves analyzing the benefits of this configuration by studying various energy management

Parameter	Notation	Unit	Value
Fixed resistances	R_0	Ω	0.000322
	R_1	Ω	0.38065
	R_2	Ω	1.3284
Fixed capacities	C_0	F	2934.7
	C_1	F	76.841
	C_2	F	1518.8
Voltage-dependent gain	k_c	F/V	130.81
Leakage resistance	R_{lk}	Ω	59436

Table 2.6: Zubieta Circuit Parameters for Supercapacitor Cell

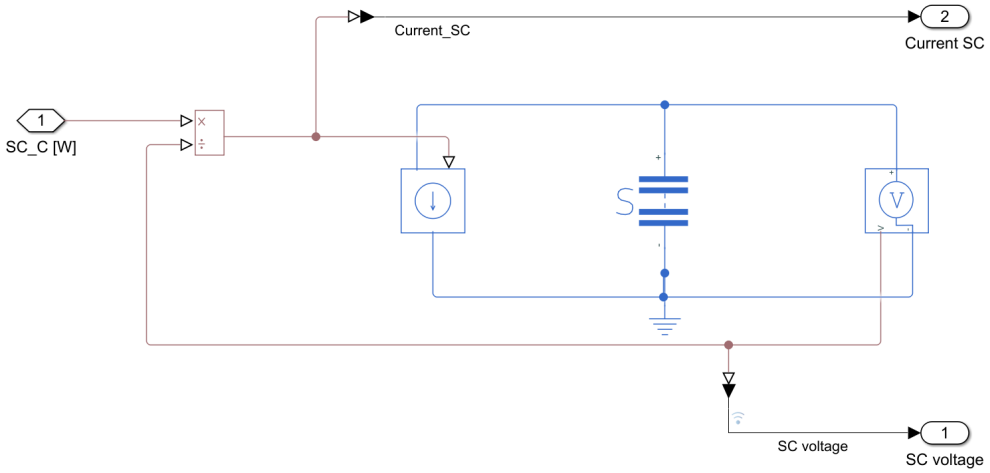

Figure 2.12: Supercapacitor Model in Simulink.

strategies and comparing their results with each other and with those obtained from a vehicle equipped only with the battery.
In a battery electric vehicle, an energy management strategy may not be necessary since the battery alone supplies all the required power at any given time. However, in a hybrid energy storage system, it becomes crucial to determine the optimal distribution of power between the available sources at every moment.
To effectively utilize the supercapacitor, it should be engaged during periods of peak power demand, thus reducing the stress on the battery. Given its lower energy density, it is important to use the supercapacitor judiciously to prevent excessive voltage drop and ensure that its stored energy is preserved for necessary high-demand instances.

2.3.1 Rule-Based Control

The initial approach to developing the energy management strategy for the hybrid electric storage system involves creating a rule-based control strategy. This strategy is designed to determine the optimal power distribution between the supercapacitor pack and the battery. The algorithm's logic is depicted in Figure 2.13.

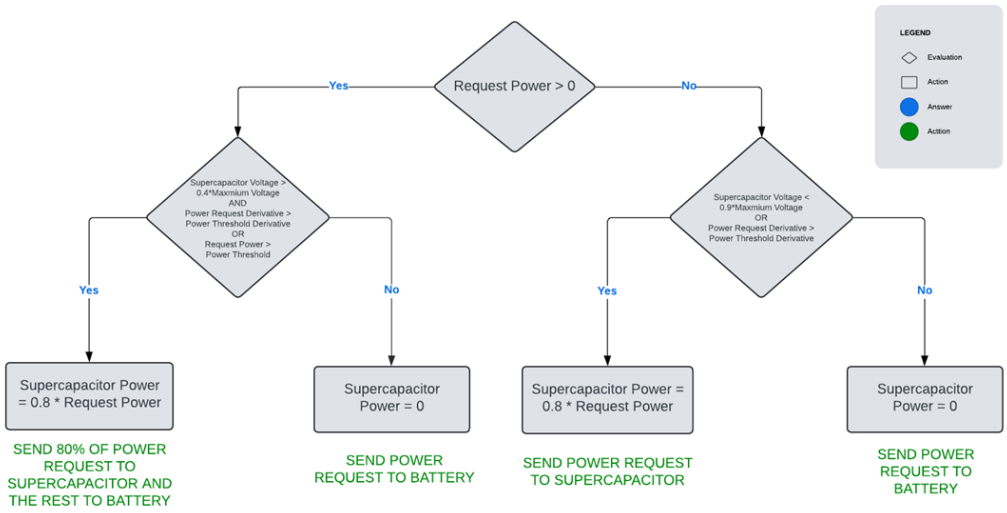

Figure 2.13: Rule Based Controller Logic Flow Chart.

The Rule-Based Controller is incorporated into Simulink via a MATLAB function block. This controller is responsible for calculating the power distribution between the supercapacitor pack and the battery based on a set of predefined rules. These rules take into account specific vehicle parameters, including the power demand from the electric motor, the rate of change of this power demand, and the voltage level of the supercapacitor. The control logic ensures that these parameters are used to determine the optimal power outputs for both energy sources.

- The power demand is monitored to ensure that the supercapacitor pack mitigates battery current spikes, thus reducing peak C-rate values.

- The power derivative acts as a trigger within the Rule-Based Control, activating the supercapacitor pack during rapid power demand fluctuations. This mechanism helps protect the battery from degradation while leveraging the quick response capabilities of the supercapacitor.

- The voltage level of the supercapacitor is continuously assessed to ensure it is only utilized when above a certain threshold. This approach ensures that the supercapacitor remains available to supply power when needed.

Supercapacitor Power Management

When the electric motor requires positive power, indicating that the vehicle is in traction, the rule-based controller draws power from the supercapacitor if either the power demand or its derivative exceeds predefined thresholds. During negative power demand scenarios, such as regenerative braking, the supercapacitor pack is prioritized for recharging over the battery if its voltage is below the upper usage limit. This prevents excessive discharge and reduces battery stress if the power derivative surpasses the threshold. To prevent rapid discharge of the supercapacitor during traction, it supplies 80% of the required power, with the remaining demand met by the battery. This method minimizes battery stress while conserving energy. Moreover, the power drawn from the supercapacitor is adjusted upwards when positive or downwards when negative, taking into account the bidirectional DC/DC converter.
The architecture of the Simulink block implementing this control logic is illustrated in Figure 2.14.

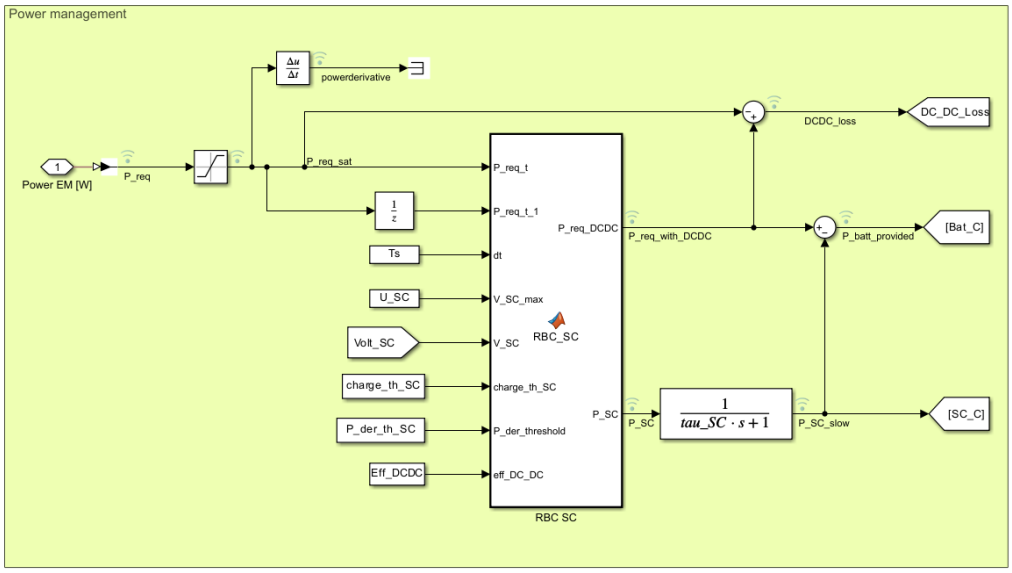

Figure 2.14: Rule Based Controller Structure in Simulink.

Supercapacitor Voltage Limits

Typically, the energy stored in a battery has a minimal impact on its voltage. In contrast, the energy stored in a supercapacitor is directly proportional to the square of its voltage. As a result, approximately 75% of the stored energy is depleted before the voltage drops to 50% of its maximum value. Therefore, in practical design applications, the maximum usable energy for a capacitor is often based on a voltage window that encompasses 50% of its total voltage range [31]. In this study, the

decision was made to charge the supercapacitor through regenerative braking up to 90% of its maximum voltage. This approach leaves room to store additional energy if the power exhibits a derivative higher than the set threshold, which could otherwise place more strain on the battery. The lower voltage limit is set at 40% of the maximum voltage to ensure maximum utilization of the stored energy.

Power Threshold Evaluation

To establish the Power Threshold value, P_{th} the power demand progression was graphed (Figure 2.15), factoring in the vehicle's mass of 13,000 kg, throughout the Manhattan drive cycle.

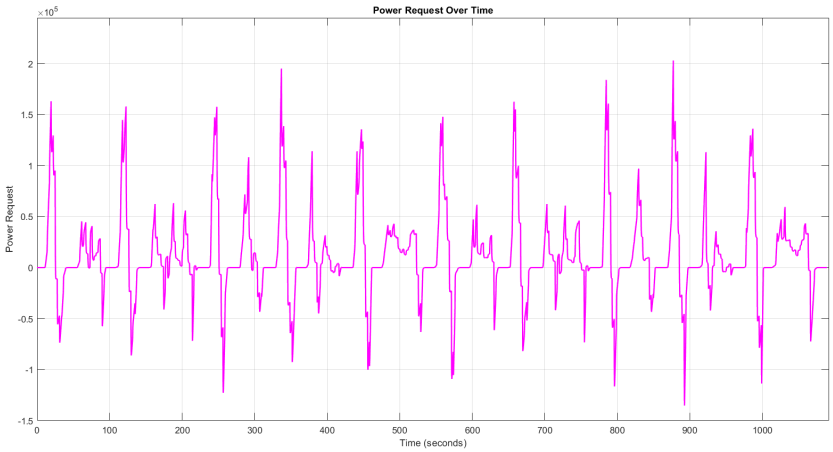

Figure 2.15: Power Request Over the Manhattan Drive Cycle for Vehicle Mass Equal to 13000kg.

It was noted that the majority of power demand peaks ranged from 60 to 160 kW. To optimize within this range, a Design of Experiments (DOE) was performed. For each Pth value, the Root Mean Square (RMS) of the battery C-rate was calculated and the results are presented in Figure 2.16.

Lower threshold values correlate with reduced battery C-rate values because the supercapacitor is utilized more frequently. However, it is crucial that the supercapacitor's voltage remains sufficient at the end of the simulation to ensure continuous operation under these conditions. Figure 2.17 illustrates the voltage trends of the supercapacitor for various selected power thresholds. Threshold values of 60, 80, 100, and 110 kW are deemed unacceptable as they indicate that the supercapacitor discharges too rapidly.

Therefore, the optimal Power Threshold value, P_{th}, which minimizes battery stress while ensuring the supercapacitor maintains adequate charge, is determined to be 120 kW.

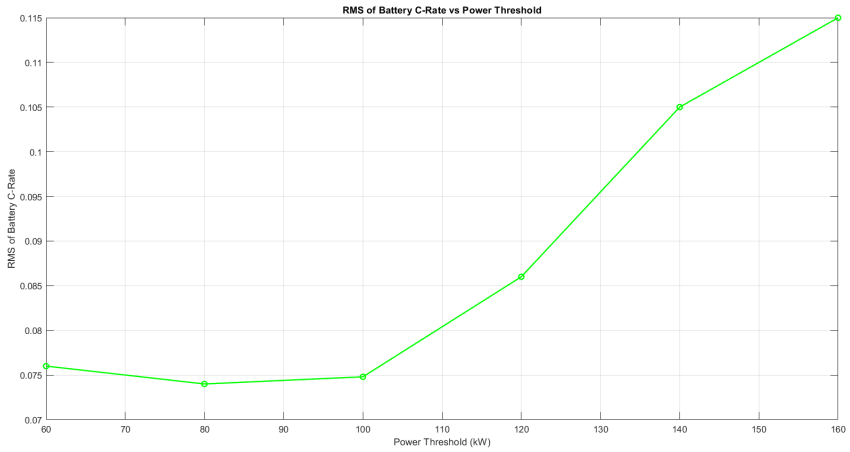

Figure 2.16: RMS of Battery C-rate Values for Various Power Threshold Values.

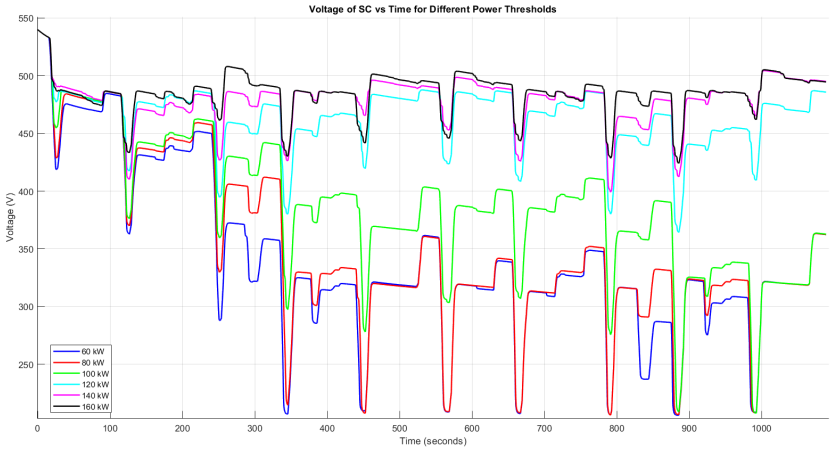

Figure 2.17: Supercapacitor Voltage During Manhattan Drive Cycle for Different Power Threshold Values.

Power Derivative Threshold Evaluation

An analogous analysis was carried out to establish the power derivative threshold, P'_{th}. Figure 2.18 presents the variation of the power derivative throughout the Manhattan drive cycle for a vehicle mass of 13,000 kg.

The figure highlights that most peaks are in the range of 10^5 W/s. Therefore, the Design of Experiments (DOE) was conducted using P'_{th} values between 10 kW/s and 100 kW/s. As in the previous analysis, the RMS value of the battery C-rate was calculated for different P'_{th} values, as shown in Figure 2.19.

It remains crucial to evaluate the supercapacitor's voltage at the end of the

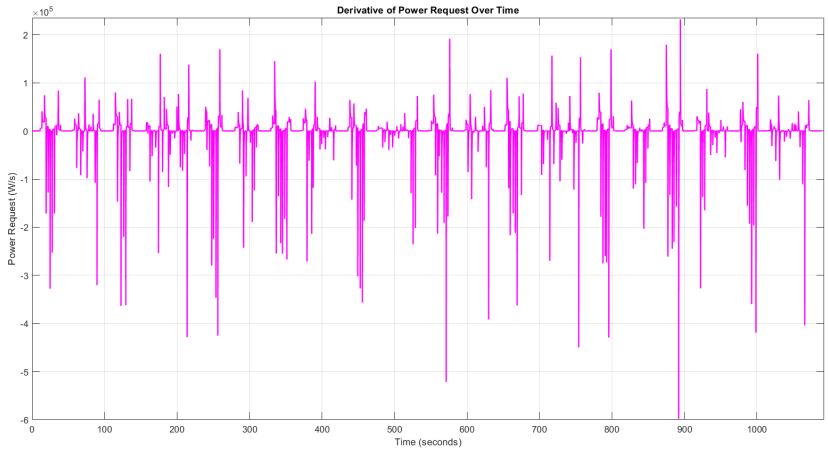

Figure 2.18: Derivative of Power Request Over Manhattan Drive Cycle for Vehicle Mass Equal to 13000kg.

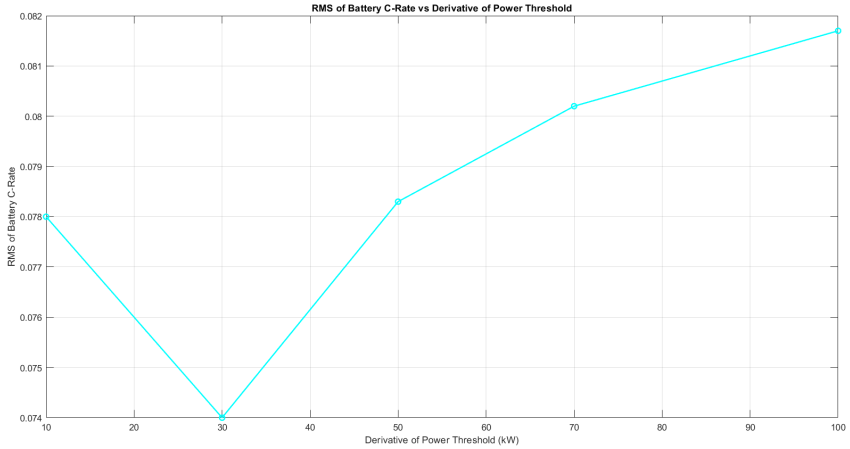

Figure 2.19: RMS of Battery C-rate Values for Various Derivative of Power Threshold Values.

simulation to ensure it maintains a charge-sustaining behavior, as illustrated in Figure 2.20.

The optimal value for P'_{th}which minimizes stress on the battery while ensuring the supercapacitor maintains the necessary charge level, is determined to be 50 kW/s.

2.3.2 Adaptive Rule-Based Control

The newly developed strategy, termed the Adaptive Rule-Based Control Strategy (A-RBC), focuses on dynamically adjusting the controller's power derivative threshold.

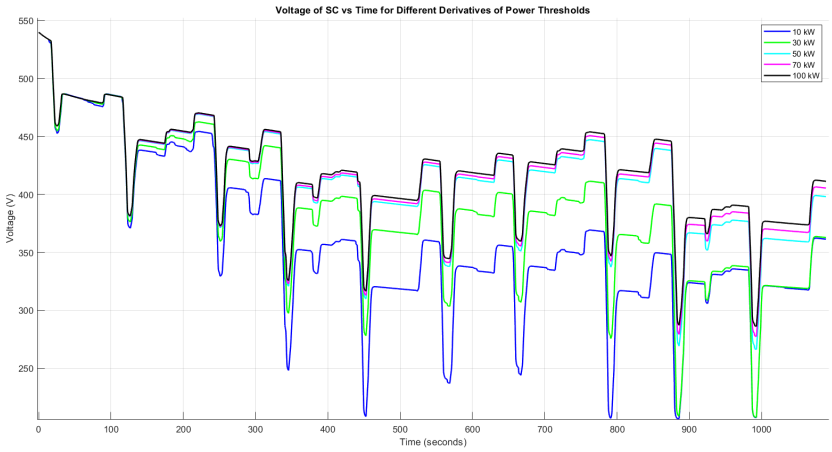

Figure 2.20: Supercapacitor Voltage During Manhattan Drive Cycle for Different Derivative of Power Threshold Values.

This adjustment is indirectly based on the power demand of the drive cycle. To make the controller adaptive, two counters are introduced, which track the frequency of the supercapacitor's utilization. Using this data, the controller can modify the threshold to optimize the use of the supercapacitor. Algorithm 1 presents the pseudocode for the A-RBC, outlining the process for calculating the new threshold value.

Algorithm 1 Adaptive Rule-Based Control Strategy

```
SET counter1 = 0
SET counter2 = 0
for each time step do
    INPUT powerRequest, voltageSC
    if powerRequest ≠ 0 then
        INCREMENT counter1
    end if
    if supercapacitor is used then
        INCREMENT counter2
    end if
    if voltageSC < 45% of maximum voltage then
        INCREMENT counter2 by 10
    end if
    COMPUTE ratio = counter2 / counter1
    COMPUTE epsilon = 10 * ratio
    UPDATE powerDerivativeThreshold = powerDerivativeThreshold * epsilon
end for
```

As the ratio rises, indicating that the supercapacitor is being used more frequently, the threshold value is increased accordingly. Conversely, a decrease in the ratio causes a reduction in the threshold value. This method allows for enhanced supercapacitor utilization in drive cycles where rule-based control would typically suggest infrequent use, thereby minimizing battery wear. The adaptive strategy lowers the power derivative threshold, promoting more frequent supercapacitor engagement in scenarios where RBC usage is limited, which helps reduce battery degradation. Conversely, in situations where RBC indicates excessive supercapacitor use, the power derivative threshold is raised to prevent over-discharge of the supercapacitor. Figure 2.21 illustrates the Simulink implementation of the adaptive rule-based control system.

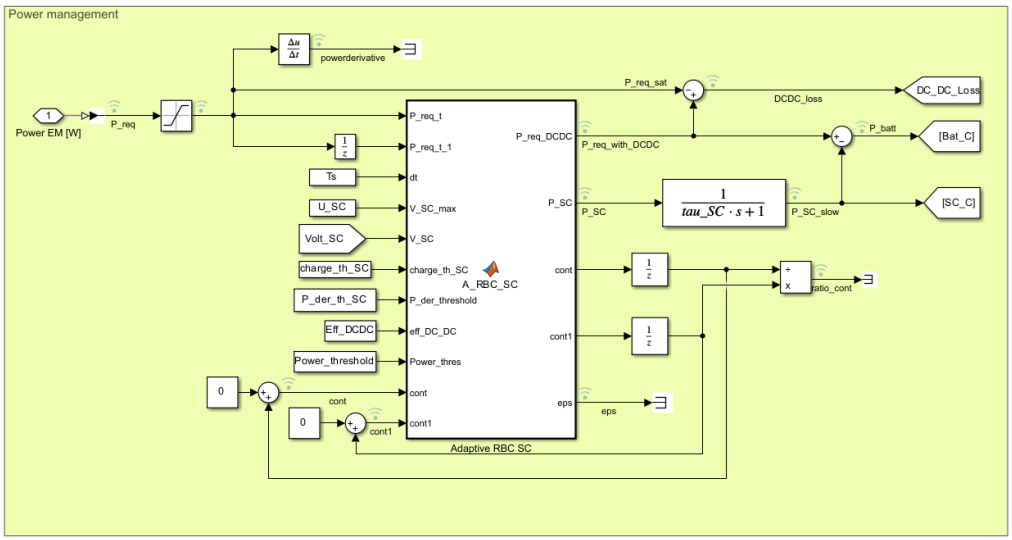

Figure 2.21: Adaptive Rule Based Controller Structure in Simulink.

2.3.3 Fuzzy Logic Control

The third energy management strategy under evaluation utilizes fuzzy logic. A Fuzzy Logic Controller (FLC) offers several benefits, including the ability to continuously manage power output from various sources and ease of design. This approach is particularly effective at capturing complex system behaviors using rules derived from expert knowledge. Additionally, the FLC allows for the straightforward integration of additional inputs, such as the vehicle's mass, to fine-tune power distribution.

Inputs of Fuzzy Logic Control

The Fuzzy Inference System has four inputs and outputs the power delivered by the supercapacitor.

1. Supercapacitor's voltage: As per Figure 2.22 , this input is divided into three membership functions:
   - **LowVoltage**: Represents a voltage lower than 215 V, which is 40% of the maximum voltage.
   - **MediumVoltage**: Covers the range between 40% and 90% of the maximum voltage.
   - **HighVoltage**: Indicates a voltage exceeding 90% of the maximum voltage.

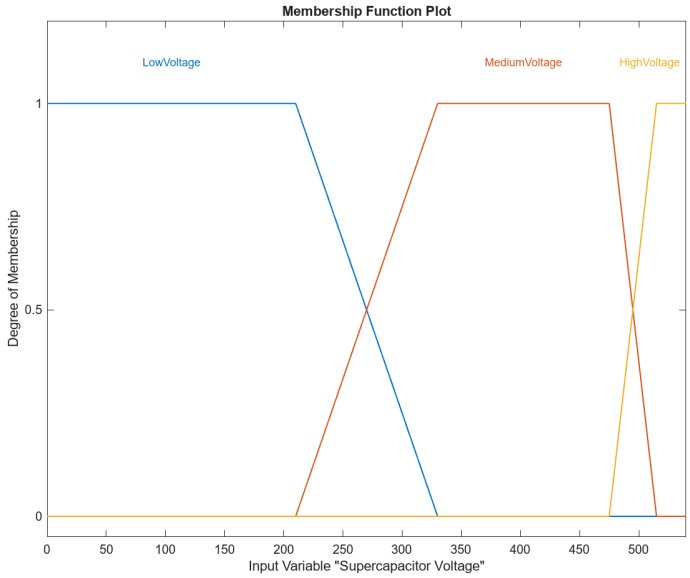

Figure 2.22: Membership Functions for Supercapacitor Voltage.

2. Power request: Refer to Figure 2.23, the power demand input is segmented into six membership functions: "NegativePower (NP)", "VeryLowPower(VLP)", "LowPower(LP)", "MediumPower(MP)" ,"HighPower(HP)" ,"VeryHighPower(VHP)". These distinct membership functions enable finer control over the output. The distribution of these membership functions is illustrated in Figure 2.23.

3. Power Derivative Request: The power derivative is categorized into three membership functions:
   - "Deceleration": Represents a negative power derivative less than -P'_{th}
   - "LowDerivative": Encompasses derivatives between -P'_{th} and +P'_{th}
   - "Acceleration": Indicates a power derivative greater than +P'_{th}

   These membership functions are detailed in Figure 2.24.

4. Vehicle Mass: The range of vehicle mass is divided into four membership functions: "LowMass", "MediumMass", "HighMass", "VeryHighMass". These membership functions are shown in Figure 2.25.

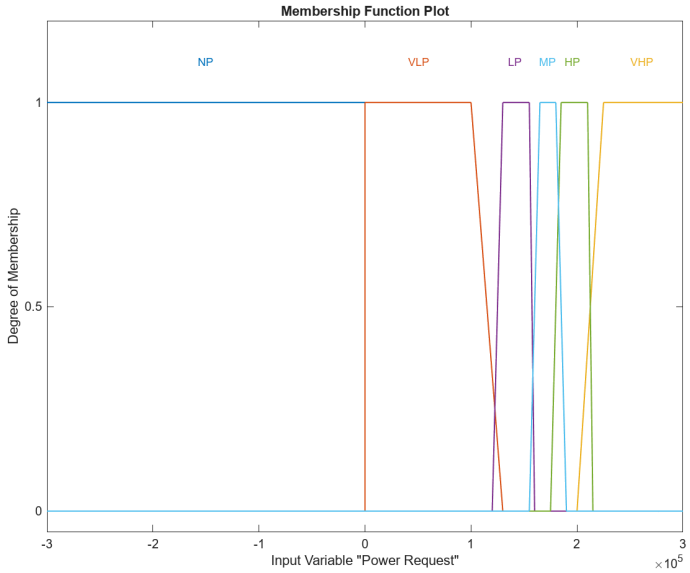

Figure 2.23: Membership Functions for Power Request.

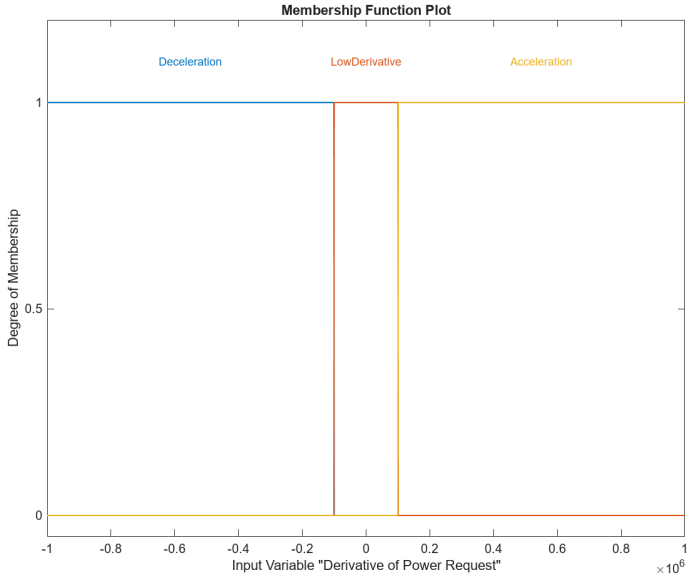

Figure 2.24: Membership Functions for Derivative of Power Request.

Output of Fuzzy Logic Control

The fuzzy logic-based energy management system produces a single output value, ranging from -1 to 1, which is divided into three categories: NegativePower, ZeroPower, and PositivePower. This output is multiplied by the absolute value of the power request to calculate the required power for the supercapacitor pack. The chosen defuzzification method is the weighted average of all rule outputs. Table 2.7

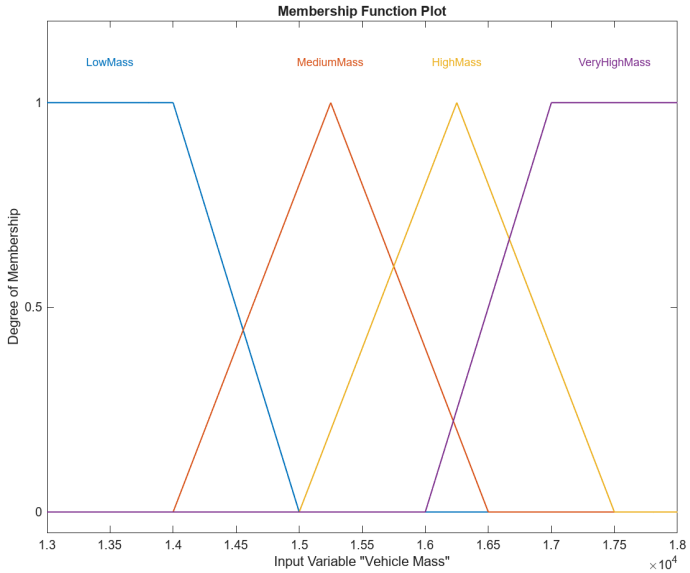

Figure 2.25: Membership Functions for Vehicle Mass.

illustrates the rules developed for this fuzzy logic controller.

Rule	Weight	Name
If voltage_sc is not HV and Power_req is NP then Power_SC is NPSC	1	Rule1
If voltage_sc is LV and Power_req is NP and Power_der is not ST then Power_SC is NPSC	1	Rule2
If voltage_sc is HV and Power_req is NP then Power_SC is ZPSC	1	Rule3
If voltage_sc is not LV and Power_req is not NP and Power_der is not ST then Power_SC is PPSC	1	Rule4
If voltage_sc is not LV and Power_req is LP and Mass is VLM then Power_SC is PPSC	1	Rule5
If voltage_sc is LV then Power_SC is ZPSC	1	Rule6
If voltage_sc is not LV and Power_req is VLP and Power_der is ST then Power_SC is ZPSC	1	Rule7
If voltage_sc is not LV and Power_req is HP and Power_der is not ST then Power_SC is PPSC	1	Rule8
If voltage_sc is LV and Power_req is VHP then Power_SC is ZPSC	1	Rule9
If voltage_sc is not LV and Power_req is MP and Mass is VLM then Power_SC is PPSC	1	Rule10
If voltage_sc is not LV and Power_req is HP and Mass is not HM then Power_SC is PPSC	1	Rule11
If voltage_sc is not LV and Power_req is LP and Power_der is ST and Mass is not VLM then Power_SC is ZPSC	1	Rule12
If voltage_sc is not LV and Power_req is MP and Power_der is ST and Mass is MM then Power_SC is ZPSC	1	Rule13
If voltage_sc is not LV and Power_req is HP and Power_der is ST and Mass is HM then Power_SC is ZPSC	1	Rule14
If voltage_sc is not LV and Power_req is HP and Power_der is ST and Mass is HM then Power_SC is ZPSC	1	Rule15

Table 2.7: Fuzzy Logic Rules

After determining the power output from the supercapacitor, the power needed from the battery is calculated by subtracting the SC pack's power contribution from the total power requirement, as depicted in Figure 2.26. In this scenario, the presence of a DC/DC converter is considered by accounting for power losses within the SC system.

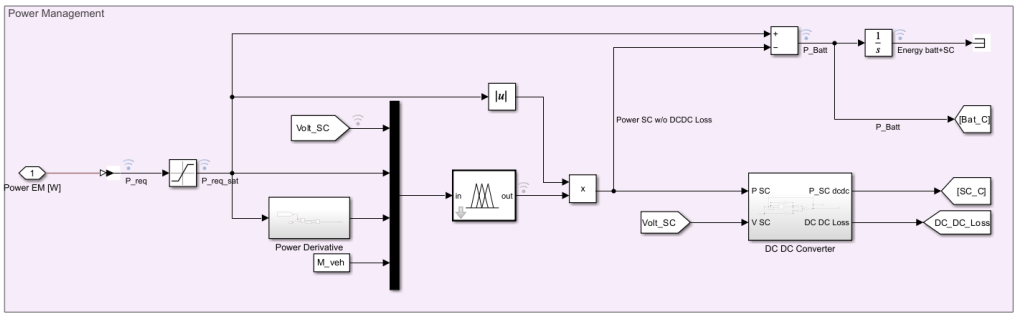

Figure 2.26: Fuzzy Logic Controller Structure in Simulink..

2.4 Simulation Result Discussion

As previously highlighted, the main goal in this initial phase of the thesis is to decrease the load on the battery by integrating a supercapacitor, thereby prolonging its lifespan. To validate and optimize this objective, the various control strategies discussed earlier will be compared:

- Battery Electric vehicle model
- Battery and SC HEV model with Rule-Based Control strategy
- Battery and SC HEV model with Adaptive Rule-Based Control strategy
- Battery and SC HEV model with Fuzzy Logic Controller strategy

The simulation results of the Battery Electric Vehicle model are utilized as a baseline. This simulation is conducted using the Manhattan bus drive cycle, previously introduced, with a vehicle mass of 13,000 kg.

2.4.1 Battery and Supercapacitor Hybrid Electric Vehicle with Rule Based Control

The simulation outcomes for the hybrid model utilizing the RBC strategy are depicted in Figures 2.27, 2.28 and are compared with the corresponding results of the BEV. The RMS relative difference of the C-rate is defined as:

$$\text{RMS}\% = \frac{\text{RMS}_y - \text{RMS}_x}{\text{RMS}_y} \times 100 \tag{2.1}$$

In this context, x and y represent scenarios with and without the supercapacitor pack, respectively. The relative differences are calculated for both the State of Charge (SOC) and the RMS values of the C-rates experienced by the battery. The summarized results are presented in Table 2.8.

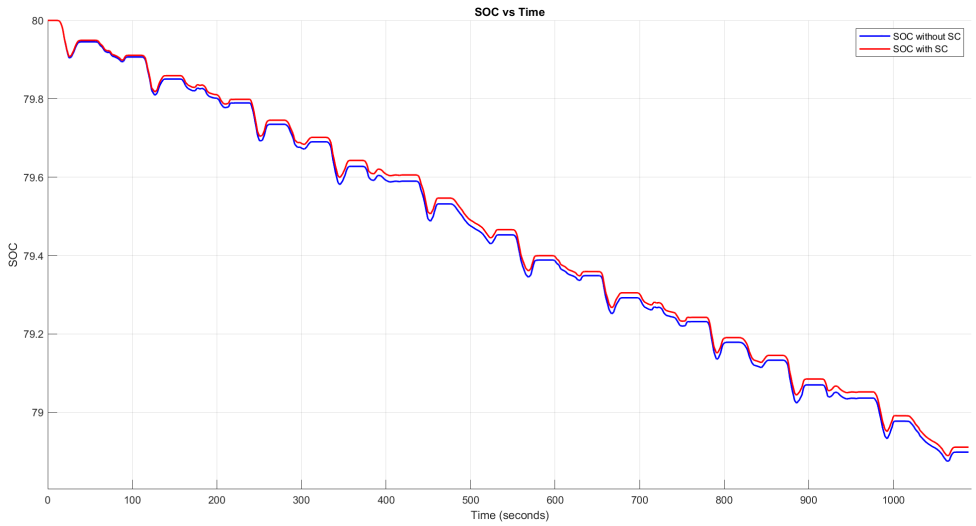

Figure 2.27: Battery SOC Evolution for BEV with and without Supercapacitor Using RBC.

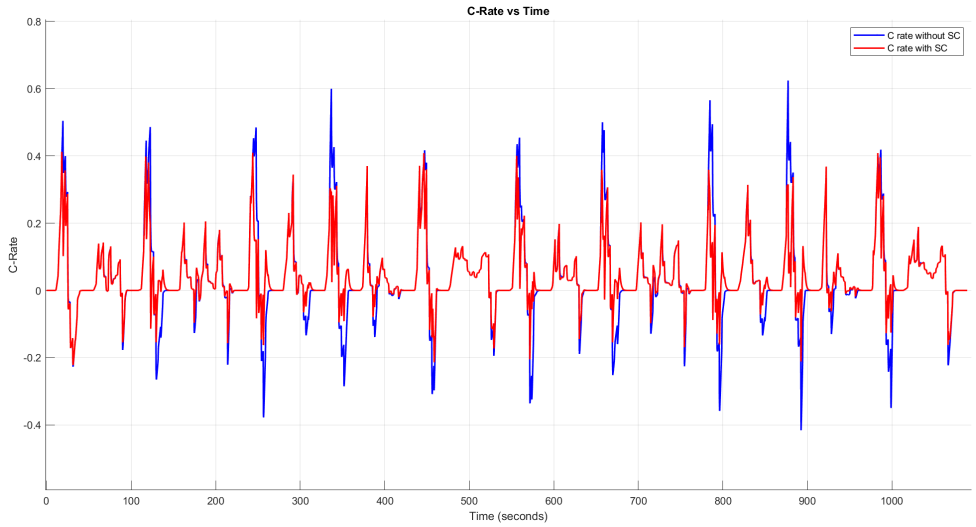

Figure 2.28: Battery C-Rate Evolution for BEV with and without Supercapacitor Using Rule Based Controller.

	BEV	**HEV**	**Relative Difference**
SOC Reduction	1.11	1.09	-1.8%
RMS of C-Rate	0.1308	0.0981	-25%

Table 2.8: Result Comparison of BEV with and without Supercapacitor

As visualized in previously mentioned figures, the addition of the supercapacitor pack does not significantly impact the battery's State of Charge (SOC), with a slight

decrease of 1.8%. This is because the energy contribution from the supercapacitor is relatively small compared to the battery due to its lower energy density. However, a substantial reduction in the C-rate is observed, with a decrease of 25%. This indicates that the supercapacitor pack effectively reduces the battery's stress during operation.

2.4.2 Comparison between Rule Base Control and Adaptive Rule Base Control Strategies

The Adaptive Rule-Based Controller (A-RBC) was designed to provide a robust energy management strategy, implemented by a rule-based controller, adaptable to various drive cycles beyond the one used for its initial optimization. To test its adaptability, both the RBC and A-RBC were evaluated using the New York drive cycle. This new cycle, described in Table 2.9, was used to determine the performance and flexibility of the A-RBC under different driving conditions.

Parameter	**Unit**	**Value**
Total cycle time	s	600
Maximum speed	m/s	12.3
Maximum acceleration	m/s^2	2.22
Covered distance	km	1.86

Table 2.9: New York Drive Cycle Data

First, the RBC and A-RBC were evaluated using the Manhattan drive cycle. The progression of the supercapacitor voltage and battery c-rate during this cycle is illustrated in Figures 2.29 and 2.30.

It can be observed that there are no significant differences, as the RBC was specifically optimized for the Manhattan drive cycle. To further evaluate the controllers, they were tested on a more demanding drive cycle, the New York drive cycle. Figures 2.31, 2.32 illustrate the supercapacitor voltage and battery c-rate trends for both controllers. In this scenario, the A-RBC adapts to the higher demands on the supercapacitor, effectively preserving its charge. The adaptive strategy optimizes the use of the SC, preventing excessive energy depletion and better managing local C-rate peaks compared to the RBC.

The graph Figure 2.33 showcases the RMS values of the C-rate experienced by the battery across various scenarios. In both scenarios, there is a reduction in the C-rates experienced by the battery. The adaptive controller maximizes the use of the supercapacitor pack, effectively assisting the battery pack.

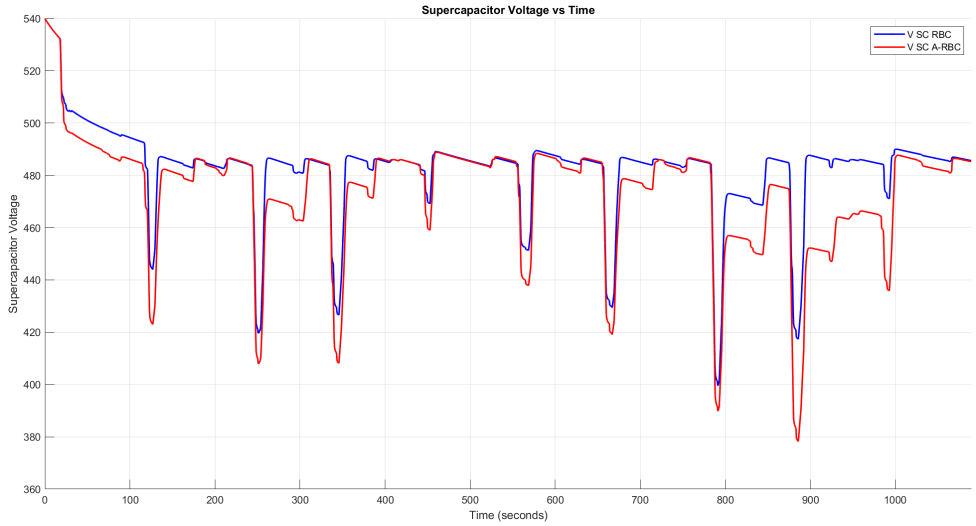

Figure 2.29: Supercapacitor Voltage Evolution Over Manhattan Drive Cycle Using RBC and A-RBC.

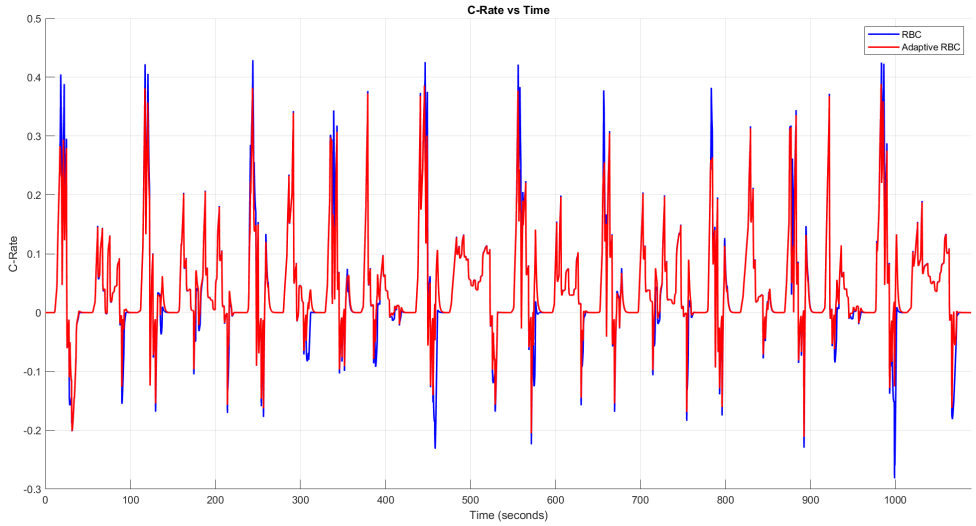

Figure 2.30: Battery C-Rate Evolution Over Manhattan Drive Cycle Using RBC and A-RBC.

2.4.3 Comparison between Rule-Based Controller and Fuzzy Logic Controller for Different Mass Values and Drive Cycle

The last energy management strategy developed is based on fuzzy logic. The idea is to create a controller that can easily adapt to variations in mass, a crucial requirement for a bus, which is constantly subject to passenger boarding and alighting. The fuzzy

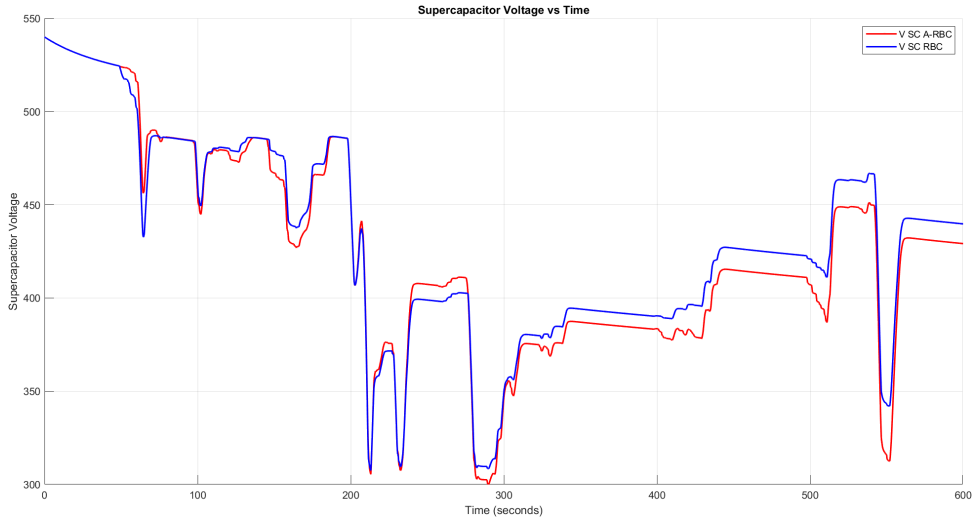

Figure 2.31: Supercapacitor Voltage Evolution Over New York Drive Cycle Using RBC and A-RBC.

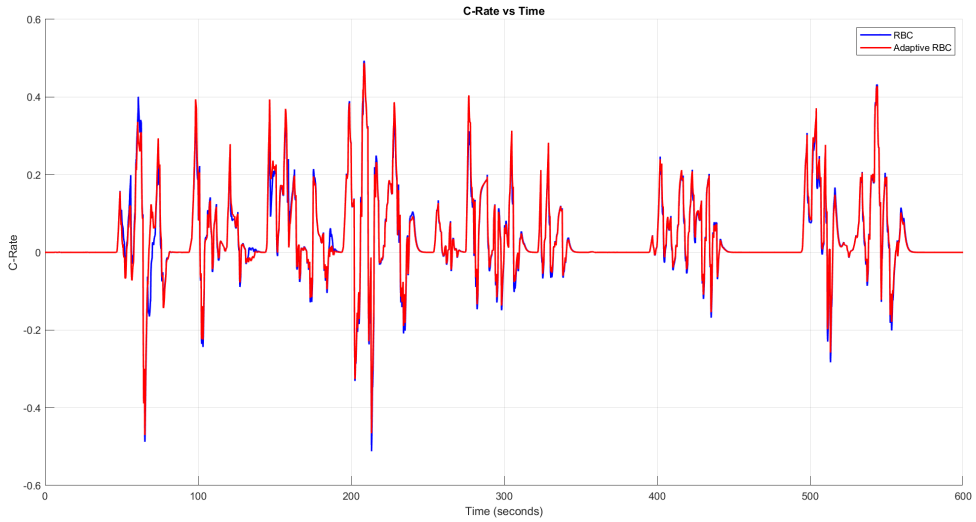

Figure 2.32: Battery C-Rate Evolution Over New York Drive Cycle Using RBC and A-RBC.

logic controller is well suited to this requirement, as it allows for the inclusion of the vehicle's mass as one of its input parameters. However, fuzzy logic does come with limitations. One significant drawback is the need for manual tuning of membership functions and rules, which can be time-consuming and requires expert knowledge. This manual tuning process can sometimes be a bottleneck, especially when dealing with highly dynamic systems where conditions change frequently and unpredictably. This limitation of fuzzy logic controller will be addressed in the following chapters.

Highlighting the key advantage of fuzzy logic, which is its capacity to deliver

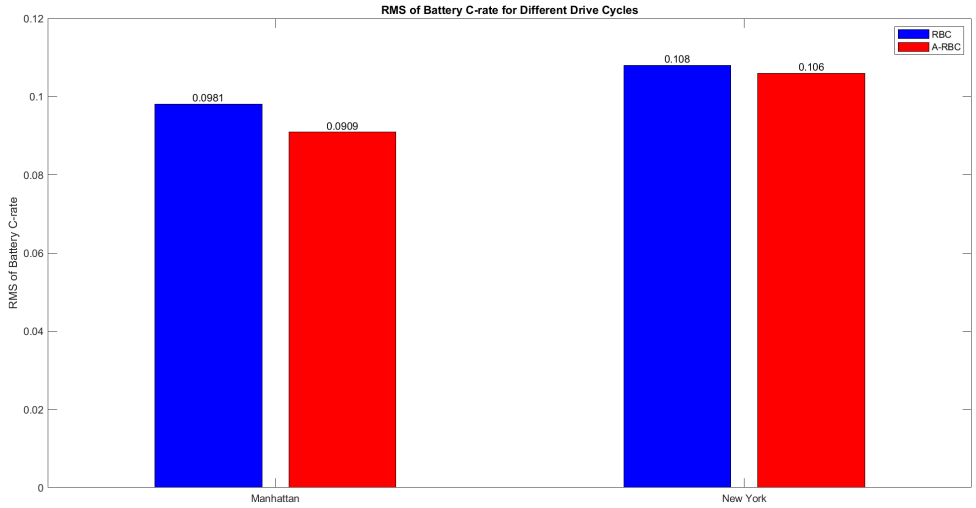

Figure 2.33: Bar Chart of the Battery C-rate RMS Values Over Different Drive Cycles for RBC and A-RBC.

smooth and continuous control signals and adaptability to varying conditions, the developed controller was simulated on the Manhattan drive cycle for three different vehicle masses: 13,000 kg, 14,000 kg, and 15,000 kg. The results were compared with those obtained from the Rule-Based control and are illustrated below, respectively in Figures 2.34, 2.35, and 2.36.

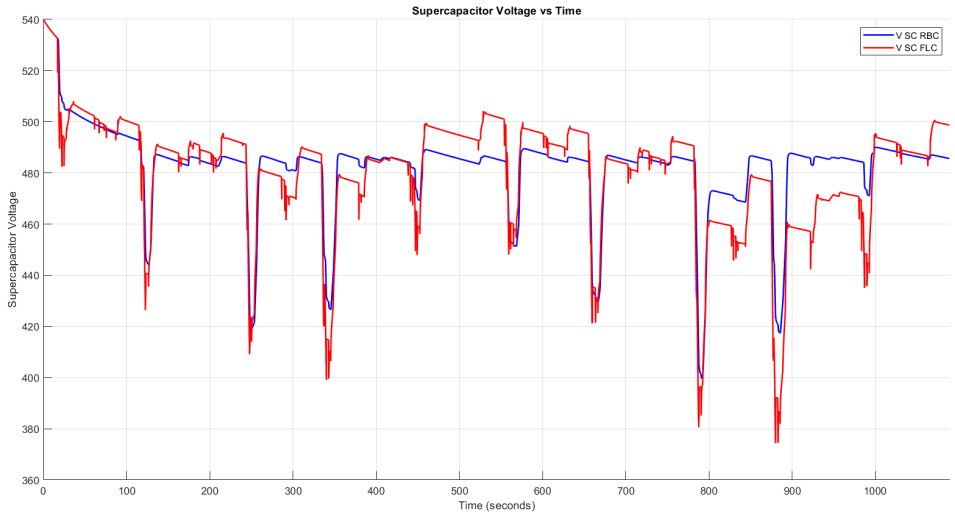

Figure 2.34: Supercapacitor Voltage Evolution Over Manhattan Drive Cycle Using RBC and FLC for Vehicle Mass Equal to 13000kg.

The Rule-Based Controller fails to efficiently utilize the supercapacitor pack when vehicle mass increases. This is evident from the very low final SC voltage at masses of

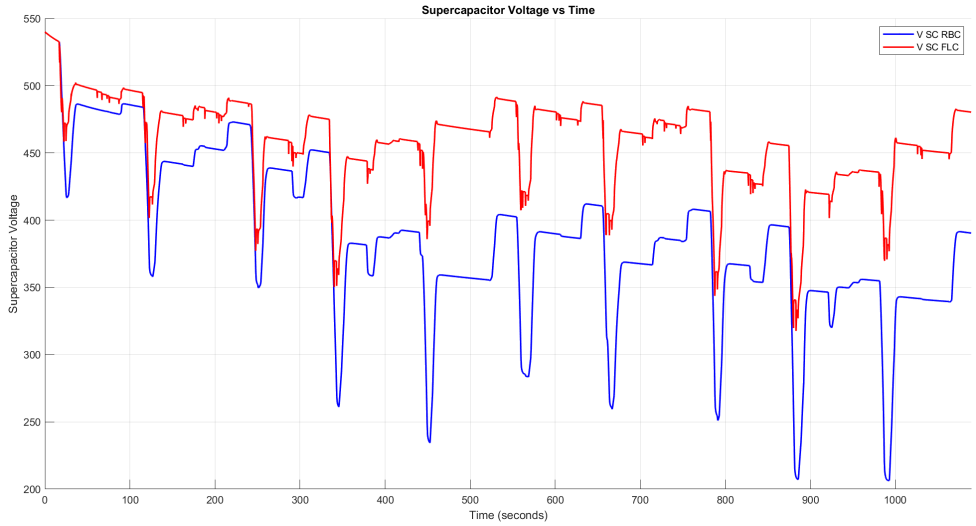

Figure 2.35: Supercapacitor Voltage Evolution Over Manhattan Drive Cycle Using RBC and FLC for Vehicle Mass Equal to 14000kg.

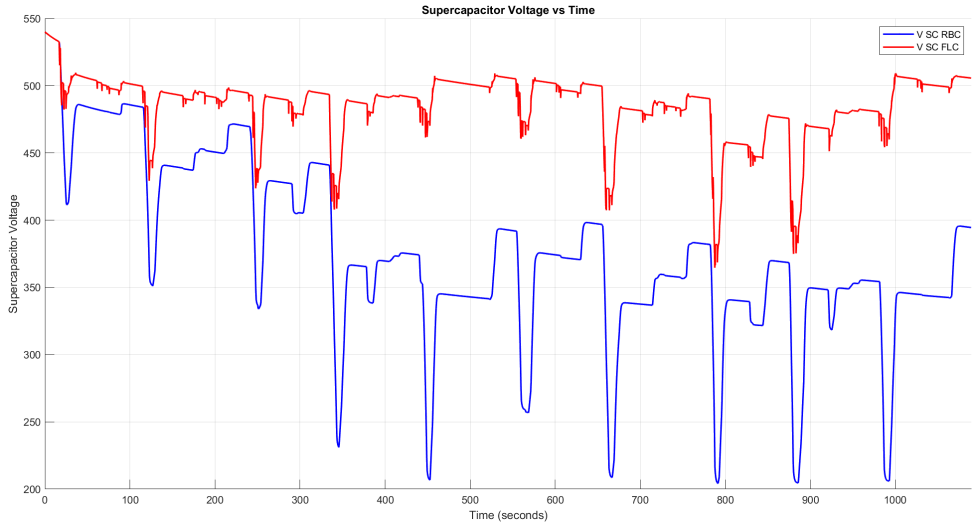

Figure 2.36: Supercapacitor Voltage Evolution Over Manhattan Drive Cycle Using RBC and FLC for Vehicle Mass Equal to 15000kg.

14,000 kg and 15,000 kg, indicating non-sustainable operation. Conversely, the Fuzzy Logic Controller adapts well to varying masses, maintaining a consistent SC voltage trend across different scenarios. Table 2.10 presents the RMS values of battery C-rates, which are higher with the Fuzzy Logic Controller. Moreover, Table 2.12 indicates the supercapacitor voltage values at the end of the drive cycle. These outcome arise because the Rule-Based Controller excessively depletes the supercapacitor, rendering it ineffective in supporting the battery in subsequent driving cycles. In

the configuration with only a battery and SC, the FLC was specifically designed to sustain the SC's charge, maintaining a high SC voltage throughout the driving cycle. While the SC voltage was well-maintained, this configuration did not significantly reduce the battery's C-rate compared to RBC. The primary reason is that with only the SC and battery, the energy demands could not be sufficiently mitigated to lower the battery's stress as the payload increased. This limitation highlighted the need for further development to achieve the desired reduction in battery C-rate.

Mass [kg]	**Battery C-Ratein RBC**	**Battery C-Ratein FLC**	**RelativeDifference**
13000	0.1027	0.0901	-12%
14000	0.0873	0.0948	+8.5%
15000	0.0950	0.112	+17%

Table 2.10: Comparison of RMS of Battery C-Rate for Vehicle Mass Varying Values Using RBC and FLC

Mass [kg]	**SC Final Voltagein RBC**	**SC Final Voltagein FLC**	**RelativeDifference**
13000	487.3	498	+2%
14000	395	480.27	+21%
15000	391.05	503.13	+28%

Table 2.11: Comparison of Final Supercapacitor Voltage for Vehicle Mass Varying Values Using RBC and FLC

The fuzzy logic-based control strategy demonstrates adaptability to different drive cycles. The model with the Fuzzy Logic Controller was simulated on the New York drive cycle and compared with the adaptive rule-based controller. Figure 2.37 illustrates the trends in supercapacitor voltage for both scenarios. This comparison highlights the FLC's ability to efficiently manage energy across varying driving conditions, showcasing its flexibility and robustness in maintaining optimal performance.

In comparison of the two control techniques in the New York drive cycle, FLC yields a slight result in managing the charge of the SC and in the battery C-rates experienced by reducing 4% the RMS of bttery c-rate, as shown in Table 2.12.

	A-RBC	**FLC**	**Relative Difference**
RMS of C-Rate	0.0986	0.0945	-4%

Table 2.12: Comparison of RMS of Battery C-Rate for A-RBC and FLC in New York Drive Cycle

The FLC efficiently manages the SC's energy, preventing rapid depletion and ensuring continuous battery support. This demonstrates the FLC's superior adaptability and effectiveness in maintaining SC charge and optimizing overall energy

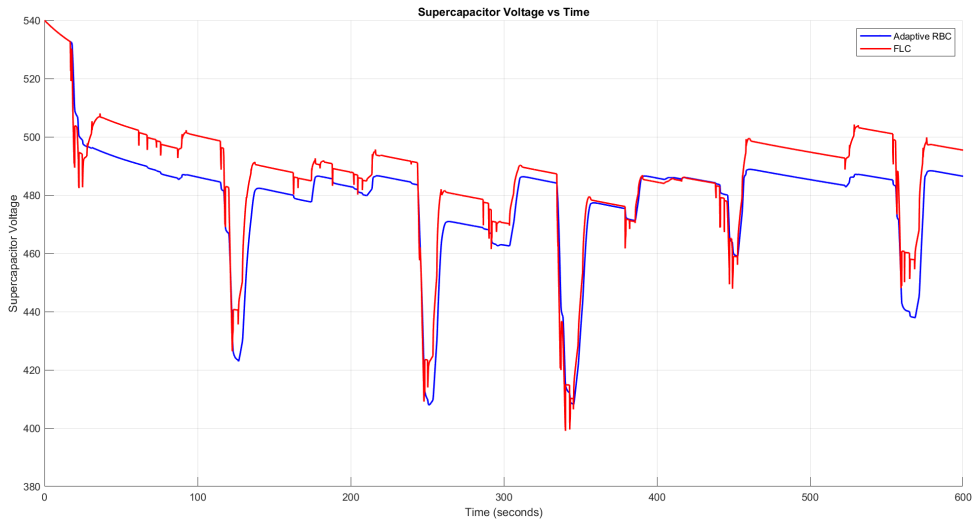

Figure 2.37: Supercapacitor Voltage Evolution Over New York Drive Cycle Using A-RBC and FLC for Vehicle Mass Equal to 13000kg.

management. However, in some cases, this approach resulted in an increased C-rate for the battery, which is undesirable. Consequently, in the next phase of the thesis, an additional energy source, Fuel Cell, was integrated into the system. This integration, along with the development of new control strategies, aimed to decrease the battery's C-rate while maintaining the SC's voltage.

Chapter 3

Fuel Cell - Battery - Supercapacitor Hybrid Energy Storage System

3.1 Fuel Cell Hybrid Electric Vehicle

The second phase of this thesis focuses on modeling and testing a hybrid energy storage system that incorporates a fuel cell stack alongside a battery pack. The objective is to significantly reduce the battery size, which in turn decreases the overall mass of the HESS. As a result, the charging rates for the new, smaller battery will be higher. To mitigate these higher charging rates, a supercapacitor pack is subsequently integrated in parallel with the battery.

3.1.1 Hybrid Energy Storage System Architecture

In this study, a modified version of topology 4, as referenced in the introduction, was selected as depicted in Figure 3.1. Unlike the original configuration where the fuel cell system supplies power directly to the load, in this setup, the fuel cell is connected in series with the battery via a DC/DC converter, and its role is to charge the battery. The battery and supercapacitors are arranged in parallel. Specifically, the supercapacitor pack is linked to the DC voltage bus through a bidirectional DC/DC converter, while the battery pack connects directly to the DC voltage bus [18].

The primary advantage of this configuration is that it allows the Fuel Cell Stack to operate continuously by charging the battery, thereby preventing fluctuations in power demand on the FCS. This helps mitigate its main drawback, which is its limited dynamic response.

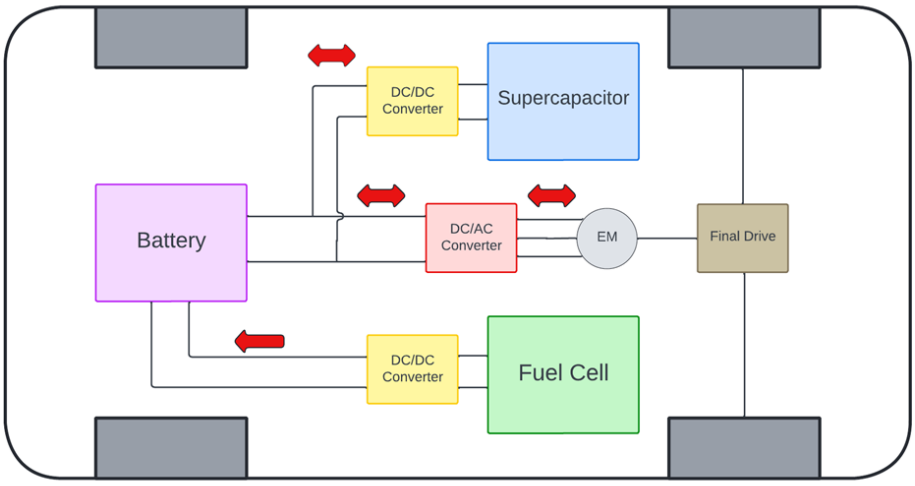

Figure 3.1: Fuel Cell Hybrid Electric Vehicle Series Configuration.

Given that one of the goals of this thesis is to reduce the battery size, a hybridization level closer to the Load Follower approach is more appropriate. The ultimate aim is to achieve a charge-sustaining mode for the battery.

This setup offers the benefit of preventing high-rate power demands on the FCS by continuously supplying power to the battery. This continuous power provision compensates for the slow dynamics of the fuel cell and reduces the C-rates experienced by the battery, thereby extending its lifespan.

3.1.2 Hybrid Energy Storage System Modelling

After determining the chosen architecture, it is essential to describe and model the involved power sources: the fuel cell stack, the battery pack, and the Supercapacitor pack, as shown in Figure 3.2. The supercapacitor pack has already been detailed in the preceding chapter and remains unchanged in this implementation, so its description will not be repeated here.

Fuel Cell Stack

The VL-40 model Fuel Cell Stack from Horizon Fuel Cell Technologies has been chosen for this research. This model was selected because the VL series is currently used to power heavy-duty vehicles in China [32]. The parameters for this Fuel Cell Stack are listed in Table 3.1.

The Simulink model of the Fuel Cell Stack relies on two lookup tables, which use a current-efficiency map and a polarization (current-voltage) map tailored for a hydrogenic power module fuel cell [33], appropriately scaled for the specific application,

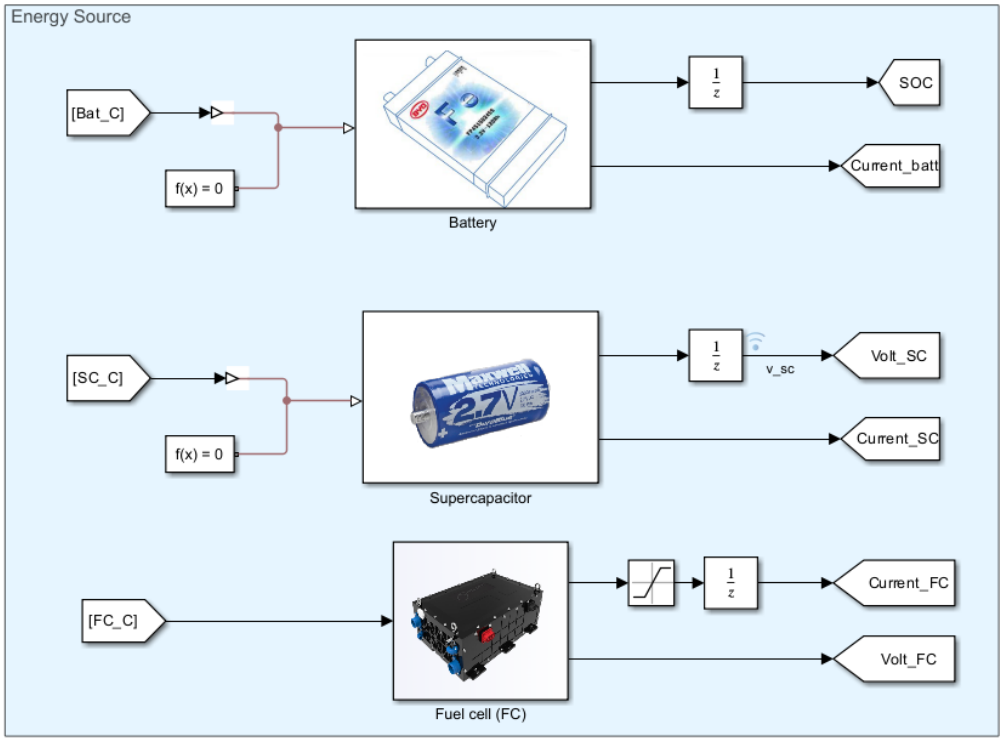

Figure 3.2: Energy Sources Structure in Simulink.

Parameter	**Unit**	**Value**
Type of Cell	-	Proton-Exchange Membrane (PEM)
Number of Cells	-	220
System Rated Power	kW	40
Voltage Output	V	145
Current Output	A	400
Ambient Temperature	°C	30-45
Working Temperature	°C	70-90
System Dimension	mm	890 x 600 x 520
Total System Weight	kg	145

Table 3.1: Fuel Cell Characteristics

as shown in Figure 3.3. Although this type of fuel cell is not identical to the selected PEM fuel cell, the overall behavior is quite similar. The current-voltage trends for both PEM and hydrogenic power module fuel cells exhibit similar patterns [34].

To verify this, the trends from the maps used in the model were compared with those provided by Horizon for a similar type of FCS, albeit smaller in size, and with data obtained from literature on PEM fuel cells.

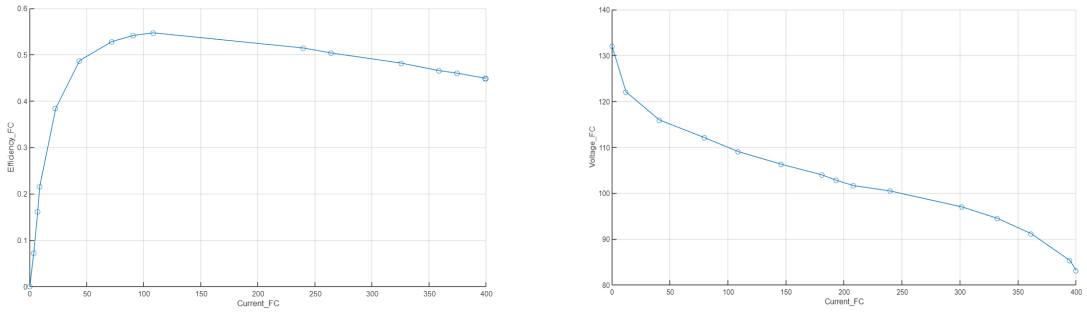

(a) **(b)**

Figure 3.3: Fuel Cell Current-Efficiency and Current-Voltage Scaled Maps.

The current-voltage map is incorporated into the Simulink model of the Fuel Cell Stack (FCS), as shown in Figure 3.4. It takes power commands as inputs and generates the corresponding voltage and current for the component.

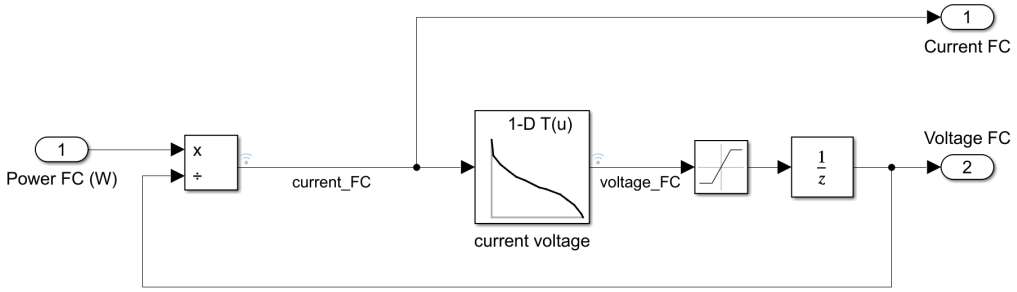

Figure 3.4: Fuel Cell Model in Simulink..

One limitation of this model is its failure to account for the sluggish dynamics of the fuel cell, which arise due to various types of losses, including activation, ohmic, and concentration losses [35]. These losses vary significantly with changes in load. According to [36], a time constant τ in a first-order low-pass filter represents the slow dynamics of the fuel cell, as follows:

$$\tau = CR_a = \frac{C(V_{\text{act}} + V_{\text{con}})}{i - i_C} \tag{3.1}$$

where V_{act} and V_{con} are respectively the voltage activation and concentration losses, and i and i_{C} are the load and capacitor currents. For this model, the specific electrochemical characteristics needed to compute this time constant, which depends on the fuel cell current, are not available. To approximate the slow response of the fuel cell stack's power delivery, a first-order transfer function with unit gain was introduced in the Simulink model at the power level, incorporating a fixed time

constant τ. The value for τ was selected based on existing literature. In [28], it was determined that a fuel cell with a rated voltage of 18.5V and a maximum current of 85A had a time constant in the order of magnitude (OOM) of $10^{-}1$ seconds. Considering that the fuel cell in this thesis has a much higher rated voltage, a more conservative approach was taken by setting the time constant to 1 second, one OOM higher than the value presented in the referenced study.

3.1.3 Hybrid Energy Storage System Sizing

Fuel Cell

To determine the suitable size for the fuel cell stack, an analysis of the energy requirements was performed. Initially, the total energy demand for the Manhattan drive cycle was calculated, as shown in Figure 3.5.

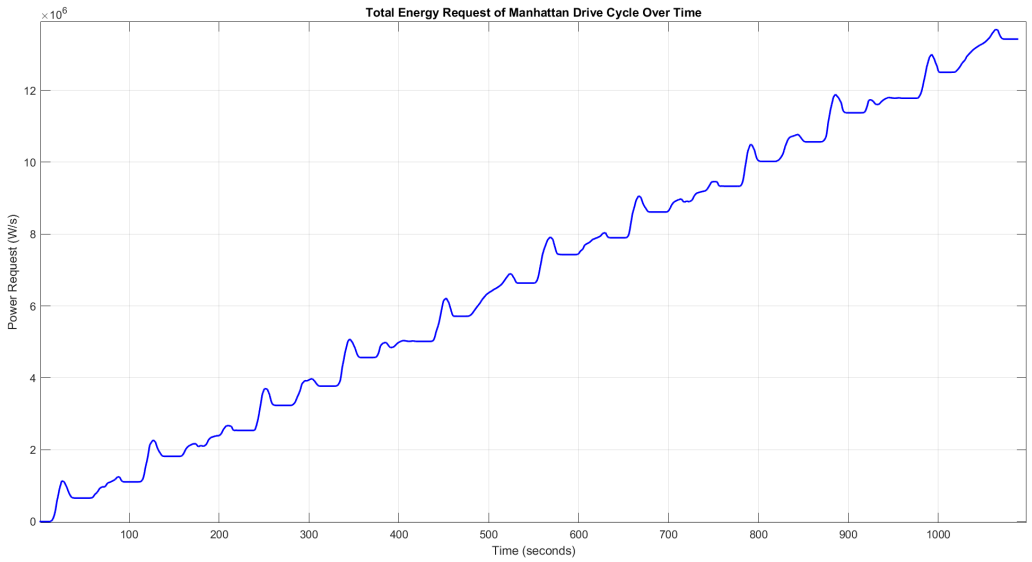

Figure 3.5: Energy Request in Manhattan Drive Cycle.

Next, the average power requirement,P_{avg} , was calculated by dividing the total energy needed for the cycle, 1.27e7 W/s, by the cycle duration of 1090 seconds. To maintain charge-sustaining operation for the battery, it was crucial to select a fuel cell stack with an output power near this average requirement. The calculation yielded an average power of 11.7 kW. Accordingly, the Horizon VL-40 fuel cell stack, which delivers a maximum efficiency output power of 12.1 kW, was chosen as it closely aligns with the average power need. Further details on the power control strategy will be discussed in the subsequent section.

Battery

Leveraging the Fuel Cell Stack (FCS) as the primary energy source enables a considerable downsizing of the battery, which now functions mainly as a power buffer. To maintain consistency in the new battery's specifications, cells identical to those used in the BYD K9 bus battery were selected for the smaller battery pack. These prismatic cells retain the same voltage but have a reduced capacity. The summarized characteristics of these cells are provided in Table 3.2.

Parameter	**Unit**	**Value**
Chemistry	-	Lithium-Iron Phosphate
Type of cell	-	Prismatic
Rated Capacity	Ah	65
Rated Voltage	V	3.2
Cell Weight	kg	1.8
Size	mm	170 x 50 x 125
Working Temperature	°C	20–60
Cycle Life	-	2000 discharge cycles ($< 1C$)

Table 3.2: Battery Cell Characteristics Used In Downsized Version

The overall voltage of the battery pack remains unchanged, thus maintaining the same configuration of 169 cells in series. However, the total capacity is reduced to one-sixth of its original value, achieved by using a single parallel row of the new cells, resulting in a capacity of 65 Ah. To calculate the mass of the new battery, the weight of a single cell is multiplied by the total number of cells in series and parallel. This calculation yields a total mass of 2081 kg. This downsizing process significantly reduces the battery's mass while ensuring it is still large enough to deliver the necessary power without rapid degradation.

3.2 Control Strategies for Energy Management

Control strategies for energy management in FCHEVs incorporating batteries and supercapacitors are crucial for optimizing performance and longevity. These strategies ensure the efficient distribution of power among the fuel cell, battery, and supercapacitor, enhancing the overall energy efficiency and reducing stress on individual components.

This section focuses on analyzing power control strategies for the fuel cell stack to ensure the battery operates in a charge-sustaining mode. This method eliminates the need for recharging the battery through a connection to the electric grid. Instead, the battery is recharged by the fuel cell and through regenerative braking, absorbing excess energy. This approach negates the need for long stops to recharge, requiring only hydrogen tank refueling.

3.2.1 Rule-Based Control

The initial approach focuses on consistently managing the power output from the fuel cell to the battery using a straightforward set of rules and incorporates two operational modes for the Fuel Cell Stack.

- Optimal Efficiency Mode: When the battery's State of Charge (SOC) is within the predefined range of 75% to 85%, the fuel cell operates at its highest efficiency point. This mode minimizes hydrogen consumption while providing the necessary power to maintain the battery's charge within this range.
- Maximum Power Mode: If the battery's SOC falls below the 75% threshold, the fuel cell switches to deliver maximum power. This rapid increase in power helps to quickly elevate the battery's SOC, ensuring it remains in a charge-sustaining condition.

Both operational points are illustrated in Figure 3.6, highlighting how the fuel cell adjusts its power output based on the battery's SOC to optimize performance and efficiency.

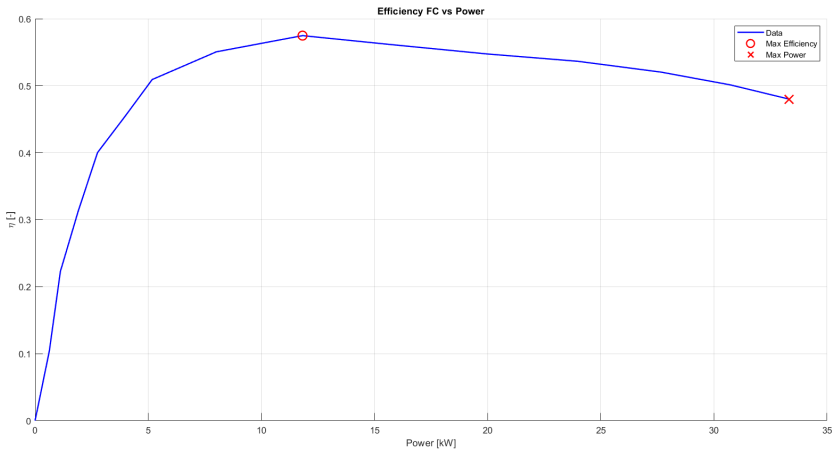

Figure 3.6: Operating Points of the Fuel Cell Stack with Rule Based Controller.

The State of Charge of the battery is maintained within the 75% to 85% range by the Rule-Based Controller. If the SOC exceeds 85%, the power generated by the Fuel Cell Stack at its maximum efficiency is halted by opening a switch. Given the fuel cell's slow dynamic response, it is more advantageous to discard the power produced when the battery SOC is above the upper limit rather than reducing the fuel cell's output to zero. This approach prevents power transients in the fuel cell, which could otherwise negatively impact its performance and stability. To implement the Rule-Based Controller in Simulink, a MATLAB function block is utilized. The flowchart depicting the RBC logic is presented in Figure 3.7.

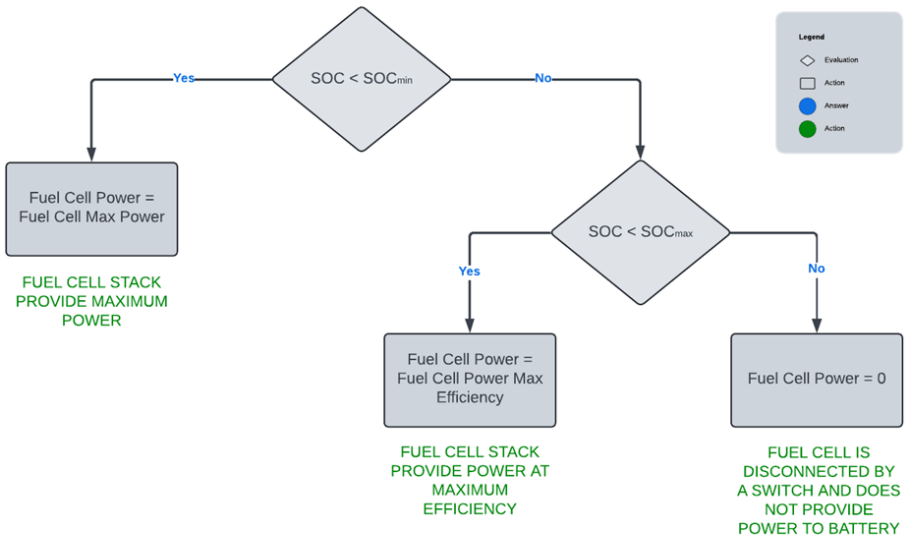

Figure 3.7: Rule Based Controller Logic Flow Chart.

3.2.2 Fuzzy Logic Control

In the previously outlined control strategy, the Fuel Cell Stack operates at two distinct points: either at maximum power or at maximum efficiency, facilitating a charge-sustaining operation. However, the fuel cell's slow dynamic response introduces challenges during transitions between these operating points, particularly when power output changes are abrupt or significant. Such rapid shifts can lead to system performance issues, such as delayed responses. To overcome this, a Fuzzy Logic-based control strategy is employed, which allows for a smoother transition between different operating points in response to varying power demands. This approach helps mitigate the impact of the fuel cell's slow dynamics, ensuring more continuous and stable power output. The operational range of the FCS under this Fuzzy Logic Control is illustrated in Figure 3.8.

The Fuzzy Logic Controller functions by generating a command that specifies the output current of the Fuel Cell. The output from the Fuzzy Inference System (FIS) block ranges from 0 to 1, where 0 corresponds to the current at the maximum power point, and 1 corresponds to the current at the maximum efficiency point. The current value is determined using two gains that are combined, as presented in Figure 3.9. For instance, if the State of Charge is near the lower limit, the FIS output might be close to 0, such as 0.2. This value is used to calculate the current at maximum efficiency, while the complement, 1-0.2 (or 0.8), is used to calculate the current at maximum power. Therefore, the resulting current is closer to the maximum power output. This approach ensures that the FC operates within the

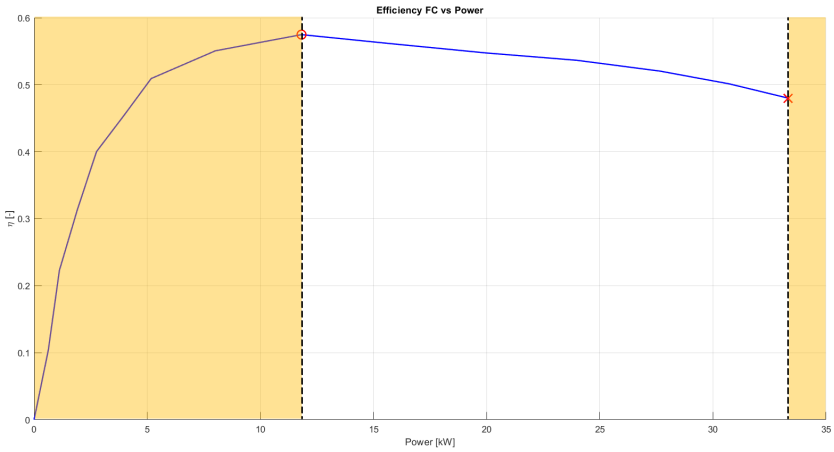

Figure 3.8: Operating Range of Fuel Cell Stack with Fuzzy Logic Controller.

range of maximum efficiency and maximum power, allowing for dynamic adjustment based on current conditions. The method ensures a smooth transition between these two points, providing a stable and efficient power output.

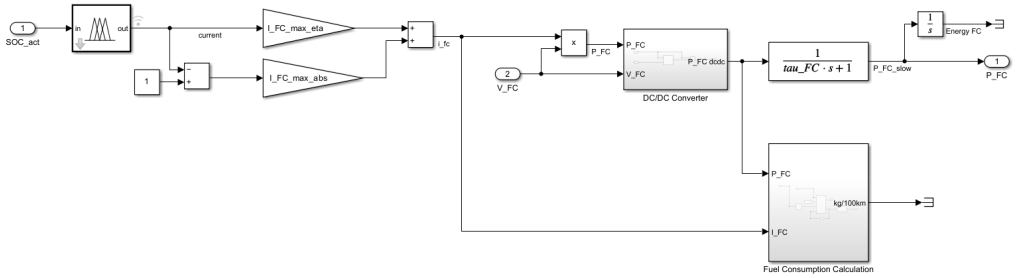

Figure 3.9: Fuzzy Logic Controller Structure in Simulink.

Fuel consumption by the Fuel Cell Stack is determined based on its efficiency at each moment, expressed in kilograms of hydrogen consumed per 100 kilometers traveled. The Fuzzy Inference System employed here is simpler than the one used for the supercapacitor in the previous chapter, featuring only one input: the battery's State of Charge. The membership functions for this input are depicted in the accompanying figure. Similar to earlier implementations, the Sugeno method was chosen over the Mamdani approach for its advantages in this context.

The input membership functions are defined as "LowSOC" and "HighSOC." "LowSOC" peaks at a State of Charge value of 75% before declining, while "HighSOC" starts increasing from the same 75% threshold, as outlined in Figure 3.10. The output, "PowerFuelCell," can assume two states: "MAX POWER" or "MAX EFF,"

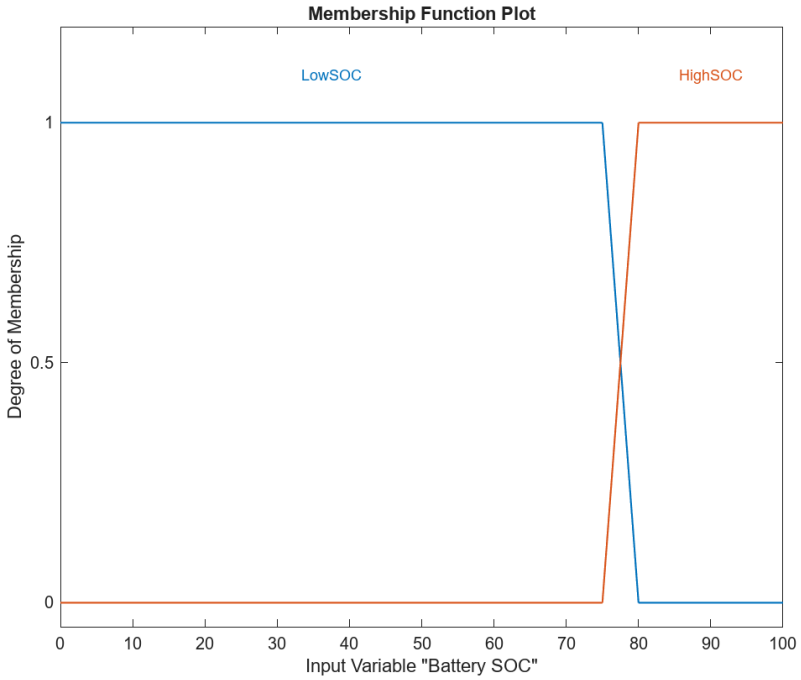

Figure 3.10: Membership Functions for Battery SOC.

corresponding to output values of 0 and 1, respectively. The rule set comprises two simple rules:

- If the battery SOC is characterized by HighSOC, then PowerFuelCell is set to MAX EFF.
- If the battery SOC is characterized by LowSOC, then PowerFuelCell is set to MAX POWER.

Moreover, the Fuzzy Logic Controller (FLC) is also employed to adjust the output power of the SC based on four key inputs: power request, supercapacitor voltage, vehicle mass, and the derivative of power request. The FLC evaluates the vehicle's power needs to determine how much power should be allocated to the SC. Figure 3.11 illustrates the surface plot showing how SC power varies with different levels of power demand and SC voltage. This input is crucial for managing the power distribution to meet the vehicle's energy requirements. The voltage level of the SC is vital for assessing its ability to supply power. Higher SC voltage indicates that the SC has more stored energy and can provide greater power output, whereas lower voltage signifies reduced available energy. The FLC uses this information to manage the SC's power output carefully to prevent excessive depletion and ensure efficient energy use.

Vehicle mass input represents the vehicle's weight, which affects the overall power demand due to variations in passenger load. The FLC adjusts the SC power in response to changes in vehicle mass to maintain optimal performance under different

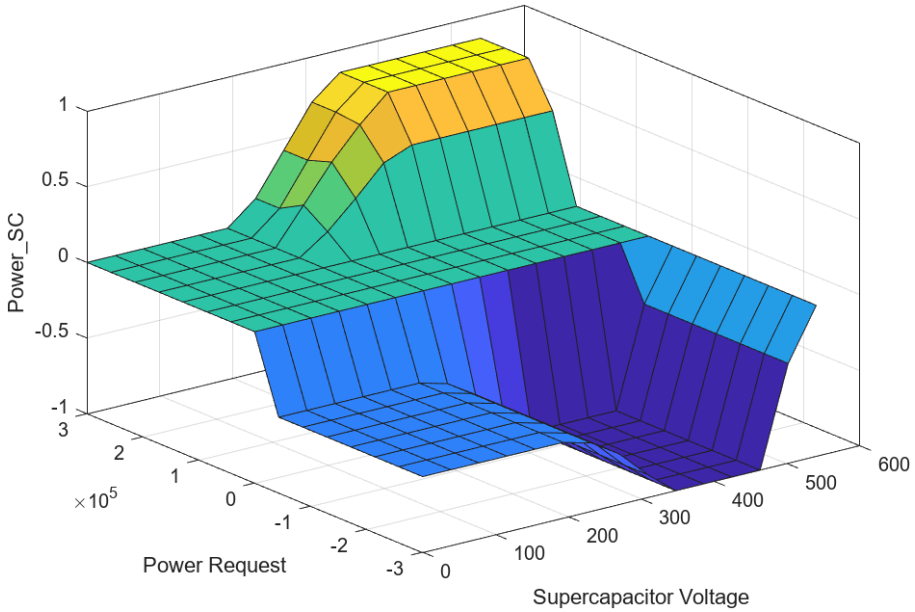

Figure 3.11: Surface Plot of Supercapacitor Power Variation with Power Demand and Supercapacitor Voltage in the Fuzzy Logic Controller.

loading conditions. Figure 3.12 demonstrates how the SC power is adjusted based on both the power request and the vehicle mass. The derivative of power request input

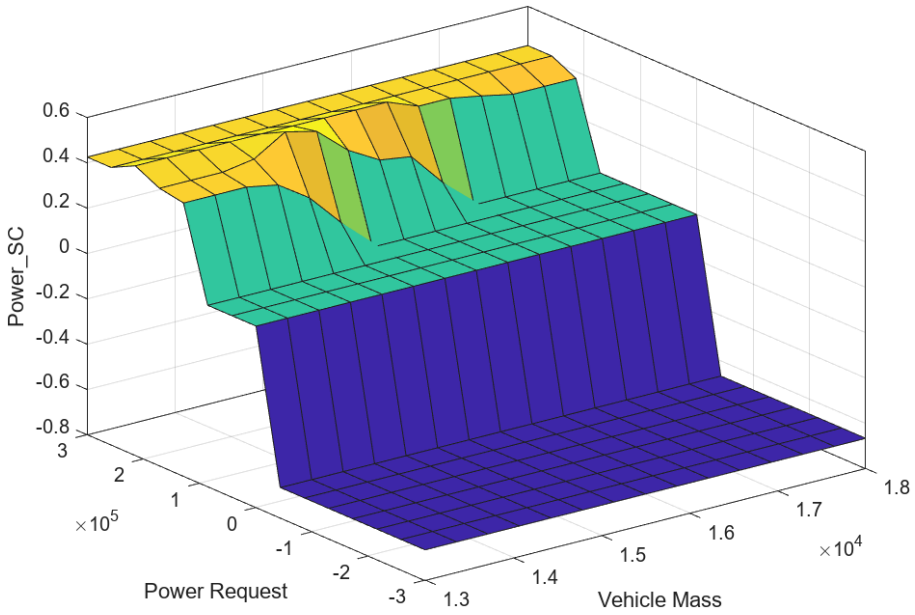

Figure 3.12: Surface Plot of Supercapacitor Power Variation with Power Demand and Vehicle Mass in the Fuzzy Logic Controller.

measures the rate of change in power demand, helping the FLC to react efficiently to sudden fluctuations. A high derivative value indicates a rapid change in power needs, requiring the SC to respond quickly to stabilize the power supply. The plot in Figure 3.13 shows how the SC power adapts to varying rates of change in power demand. Through the integration of these inputs, the FLC effectively manages the

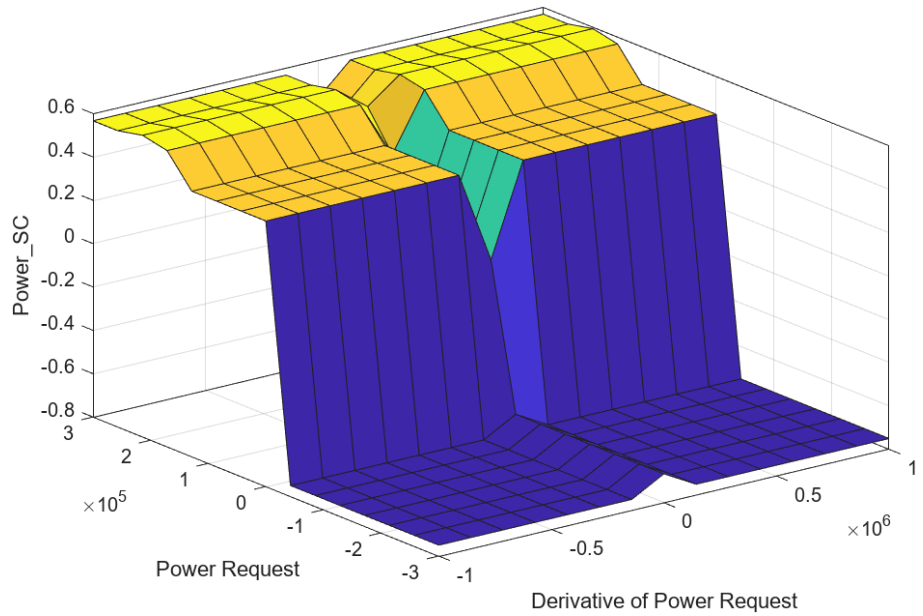

Figure 3.13: Surface Plot of Supercapacitor Power Variation with Power Demand and Its Derivative in the Fuzzy Logic Controller.

SC's power output to balance the energy demands of the vehicle, reduce battery stress, and optimize overall energy management.

3.2.3 Adaptive Neuro-Fuzzy Inference System

To address the dynamic and complex requirements of a hybrid electric vehicle's energy management system, this thesis employs the Adaptive Neuro-Fuzzy Inference System (ANFIS). ANFIS excels in handling nonlinear relationships between vehicle parameters such as vehicle mass, power demand, and state of charge. This capability is particularly vital for buses, which experience significant changes in passenger load throughout their daily routes.

Additionally, ANFIS provides precise control and efficiency in managing power distribution between the battery, supercapacitor, and fuel cell. Its ability to make accurate predictions and adjustments helps to optimize energy usage, reduce wear on components, and improve overall system efficiency.

The table 3.3outlines the qualitative and quantitative advantages of ANFIS over traditional fuzzy logic systems, highlighting how ANFIS improves learning capability,

adaptability, optimization, and performance metrics.

Aspect	Fuzzy Logic	ANFIS	Type
Learning Capability	Requires manual setup and expert knowledge	Automatically learns and adjusts rules from data	Qualitative
Adaptability	Uses static rules and membership functions	Adapts to changing conditions through continuous learning	
Optimization	Manual tuning is time-consuming and may not be optimal	Uses hybrid learning algorithms for better performance	
Handling Nonlinearities	Struggles with complex systems	Neural networks enhance modeling of complex relationships	
Scalability	High complexity with more input variables	Efficiently handles higher-dimensional input spaces	Quantitative
Improved Performance Metrics	Incremental improvements, limited impact on system wear	Fine-tunes control strategies for better real-time performance	

Table 3.3: Comparison of Fuzzy Logic and Adaptive Neuro-Fuzzy Inference System

Training and validation phase of ANFIS

To prepare the neural network model, the input and output data collected from these FLC simulations are used as outlined in table 3.4. The process begins with gathering training data from simulations using a Fuzzy Logic Controller. In these simulations, the vehicle mass is varied to mimic real-world scenarios where passengers enter and exit the vehicle. This dynamic change in mass directly impacts the energy management requirements, making it essential for the ANFIS model to learn how to adapt effectively.

An integral part of this training phase is data augmentation. By artificially expanding the training dataset, the model is exposed to a broader range of scenarios, ensuring it can handle various mass changes and optimize the use of supercapacitors more effectively, especially under high mass conditions. This enhanced learning process helps the ANFIS model generalize well and maintain performance consistency across different operational states.

Manhattan driving cycle duration [s]	Vehicle Mass [tons]	No. Passengers
0-272	14.554	21
273-544	13.518	7
545-816	14.036	14
817-1089	15.072	28
1090-1361	13.740	10
1362-1633	14.406	19
1634-1905	13.222	13
1906-2177	13.592	8
2178-2449	14.702	23
2450-2721	14.998	27
2722-2993	14.850	25
2994-3267	14.924	26

Table 3.4: Training and Validation Data of Adaptive Neuro-Fuzzy Inference System.

3.3 Simulation Result Discussion

3.3.1 Hybrid Energy Storage System Mass and Range Consideration

The original vehicle configuration, a battery electric vehicle (BEV), was simulated to determine the baseline range. This simulation, using a battery-only model, yielded a range of 305 km. The battery specifications for this model were 600 Ah capacity and 540 V, resulting in a total energy capacity of 324 kWh. To determine the energy consumption rate, the total energy capacity was divided by the range, resulting in an energy consumption rate of approximately 1.0623 kWh per kilometer.

To maintain the same vehicle range of 305 km after integrating additional energy sources such as a fuel cell and a supercapacitor, it is essential to precisely calculate the new required battery capacity. This process involves several steps to ensure that the energy demands of the vehicle are met while optimizing the battery size.

The chosen fuel cell, the VL-40, was selected based on the goal of achieving charge-sustaining operation for the battery. This means that the fuel cell stack was chosen with output power at maximum efficiency close to the average power required by the drive cycle. The effective hydrogen consumption rate of the VL-40 is 0.1372 kg per kWh, calculated considering an average hydrogen consumption of 0.73 cubic meters per kWh and an efficiency of 47.8%. Given a hydrogen storage capacity of 10 kg, the energy capacity provided by the fuel cell is approximately 72.89 kWh.

The supercapacitor pack is composed of 200 cells in series, each with a voltage of 2.7 V and a rated capacitance of 3000 F. The total capacitance of the supercapacitor pack is 15 F, and the total voltage is 540 V. The energy capacity of the supercapacitor

pack is approximately 0.608 kWh. The combined energy contribution from the fuel cell and supercapacitor is therefore 73.498 kWh. This combined energy contribution is subtracted from the total energy required to maintain the same range of 305 km, resulting in a new required battery energy of approximately 250.502 kWh.

Finally, the new battery capacity is calculated based on the required battery energy and the battery voltage. The new required battery capacity is approximately 464 Ah. By integrating the VL-40 fuel cell and the supercapacitor into the hybrid energy storage system, the battery capacity can be downsized to approximately 464 Ah while maintaining the same range of 305 km. This downsizing is achieved by leveraging the additional energy contributions from the fuel cell and supercapacitor, ensuring that the vehicle's energy demands are met efficiently. This approach not only optimizes the energy storage system but also enhances the vehicle's overall performance and range sustainability.

The mass of the Hybrid Energy Storage System (HESS), which includes the Fuel Cell stack, Battery, and Supercapacitor working in synergy, is calculated by summing the individual masses of these components. The mass of the baseline system, consisting of the original 600Ah battery, is 3118 kg (calculated as 169 cells in series, 3 in parallel, each cell weighing 6.15 kg). In the HESS configuration, the downsized battery mass is 2081 kg (169 cells in series, 2 in parallel, each cell weighing 6.15 kg, plus 169 cells in series, 1 in parallel, each cell weighing 1.8 kg). Adding the masses of the Fuel Cell (145 kg) and the Supercapacitor (95 kg), the total mass of the HESS is 2623 kg, representing a 15% reduction in weight, as detailed in Table 3.5.

Configuration	Battery Capacity	SC Capacity	FC Capacity	Range	Mass	Mass Reduction	Energy Reduction
Baseline BEV	600 Ah – 324 kWh	-	-	305 km	3118 kg	-	-
Streamlined HESS EV	465 Ah – 251 kWh	0.608 kWh	72.89 kWh	305 km	2623 kg	15%	22%

Table 3.5: Comparison of Baseline BEV and Streamlined HESS EV Configurations

3.3.2 Comparison of Rule-Based and Fuzzy Logic Controllers with Battery and Fuel Cell Integration

To compare the implemented strategies, we considered the battery State of Charge, which needs to remain within the 75-85% range to operate in charge-sustaining mode, and the fuel consumption.

Figure 3.14 illustrates the SOC (State of Charge) and FC (Fuel Cell) power trends over time for the two different controllers. It can be observed that the rule-based strategy struggles to maintain the battery charge level around the desired target of 80%, showing a decreasing trend instead. Although the Fuzzy Logic Controller exhibits higher fuel consumption, this is due to its ability to adjust power output in response to SOC variations, increasing output when necessary. This adjustment results in a slight deviation from the maximum efficiency point, leading to increased hydrogen consumption.

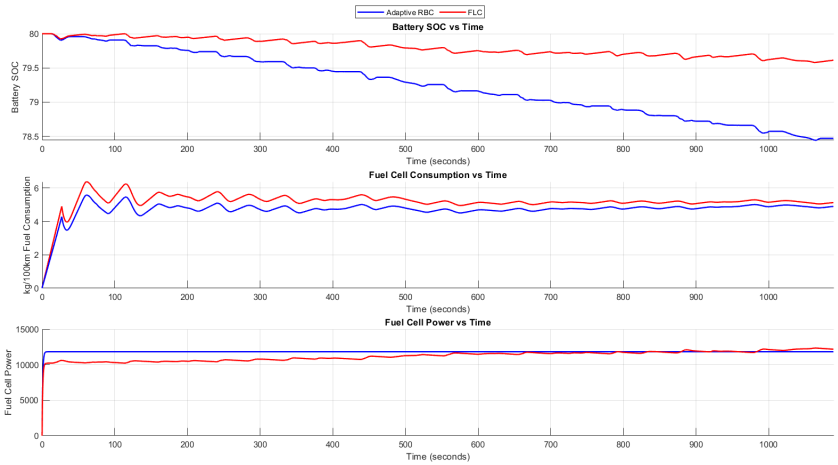

Figure 3.14: Battery SOC, FC Fuel Consumption and Power Comparison for RBC and FLC, with initial SOC Equal to 80%

Additionally, it is crucial to compare the two strategies when the SOC falls below the threshold value, causing the ARBC-controlled fuel cell to change operating conditions. For this comparison, the initial SOC was set to 74%, just below the 7% threshold. The results of this scenario are presented in Figure 3.15.

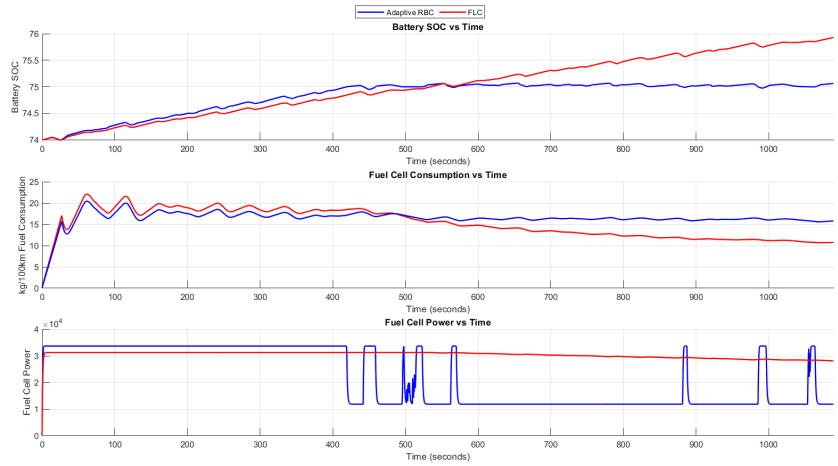

Figure 3.15: Battery SOC, FC Fuel Consumption and Power Comparison for RBC and FLC, with initial SOC Equal to 74%

In this scenario, the FCS controlled by the adaptive Rule-Based Controller (ARBC) oscillates between two working points, resulting in a highly discontinuous power trend. This behavior is undesirable as the fuel cell cannot rapidly adjust its output power, leading to performance issues. Conversely, the fuzzy logic-based strategy ensures a

continuous power output from the FC, which is more favorable. The SOC of the battery increases towards the target value under the FLC, while the ARBC fails to charge the battery effectively. Although the FLC has higher fuel consumption due to greater power generation during the simulation, this trade-off leads to improved battery performance. The results are summarized in Table 3.6, where the relative differences have been calculated to facilitate qualitative interpretation.

		Final SOC	**SOC difference**	**FCFuel Consumption**
SOC initial = 80	**ARBC**	78.4	-1.6	5.1
	FLC	79.7	-0.3	5.4
	Relative Difference		+81%	+5.8%
SOC initial = 74	**ARBC**	75.2	1.2	15.1
	FLC	75.9	1.9	11.3
	Relative Difference		+58%	-25%

Table 3.6: Absolute Values and Relative Differences of Battery SOC and Fuel Consumption between the reference RBC and the FLC

3.3.3 Analysis of C-Rates and Supercapacitor Integration in Battery and Fuel Cell Configurations.

The smaller-sized battery has reduced the overall mass of the Hybrid Energy Storage System. However, its lower capacity results in higher C-rate values due to the currents flowing through it. Simulations on the Manhattan drive cycle show battery C-rate peaks exceeding 0.7C several times. These C-rate values, even for short durations, can accelerate battery degradation and shorten its lifespan. Increasing the battery size could mitigate this issue but would partially offset the mass reduction benefits. Instead, a supercapacitor, identical to the one described previously, was introduced. The SC is connected in parallel to the battery and in series with the fuel cell. It provides power during high demand or rapid fluctuations and absorbs power during regenerative braking, prioritizing over the battery. The battery, however, is continuously recharged by the FCS, with the connection opening only if its SOC exceeds a predefined threshold, allowing the FC to recharge the SC pack. This simple power distribution strategy for the FCS between the battery and SC is summarized in the pseudocode shown in Algorithm 2. Figure 3.16 illustrates the comparison of the battery's C-rate trends with and without the supercapacitor integration.

The presence of the supercapacitor reduces the peak C-rate experienced by the battery, consistently keeping it below 0.5C. Additionally, by absorbing power from regenerative braking, the SC greatly diminishes the negative current passing through the battery, thereby further reducing the stress it endures.

To facilitate a qualitative comparison, table 3.7 presents the RMS values of the battery's C-rate and their relative differences.

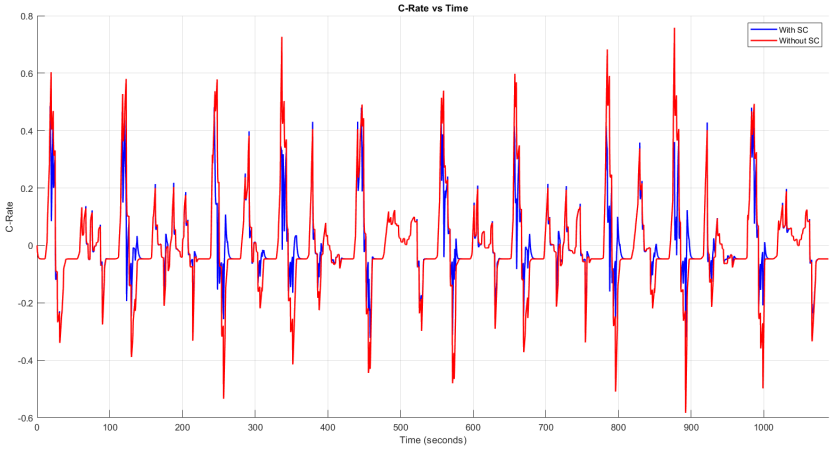

Figure 3.16: Battery C-rate Comparison Between HESS with and without Supercapacitor.

Algorithm 2 Pseudocode for Power Management

READ VoltageSupercapacitor, SOCactual, PowerFuelCell, MaxVoltageSC
SET SocUpperBound = 85%
SET VoltageSCUpperBound = 90% MaxVoltageSC
if SOCactual is less than SocUpperBound **then**
    PowerFCtoBattery = PowerFuelCell
    PowerFCtoSC = 0
else if VoltageSupercapacitor is lower than VoltageSCUpperBound **then**
    PowerFCtoBattery = 0
    PowerFCtoSC = PowerFuelCell
else
    PowerFCtoBattery = 0
    PowerFCtoSC = 0
end if
END

	Without SC	**With SC**	**Relative Difference**
RMS of C-Rate	0.1622	0.1099	-32%

Table 3.7: Result Comparison of FCHEV with and without Supercapacitor

3.3.4 Comparison of Rule-Based and Fuzzy Logic and ANFIS Controllers with Battery and Supercapacitor and Fuel Cell Integration

ANFIS demonstrates its advantage in managing the nonlinear relationships between vehicle parameters, especially vehicle mass. This capability is crucial for buses, which face significant variations in passenger load throughout their daily operations. This section presents the simulation results for various vehicle mass values, illustrating how energy usage was optimized. The use of SC and FC effectively reduced the wear and C-rate of the battery.

In this phase, the system was enhanced by introducing a fuel cell and supercapacitor, creating a hybrid energy system with the SC, FC, and battery. With this new configuration, the Fuzzy Logic Controller was adjusted to allow more aggressive use of the SC. As a result, the SC voltage decreased more than in the previous chapter. However, this increased utilization of the SC led to a greater reduction in the battery's C-rate and improved State of Charge. The FC's presence compensated for the SC's increased usage, providing a continuous power source and further reducing battery stress. The results demonstrated that the FLC, by effectively leveraging the additional energy source, achieved the primary goal of reducing the battery's C-rate. The increased use of the FC under the FLC strategy compared to the RBC supported this outcome, aligning with the overall objective of enhancing the system's energy management and efficiency.

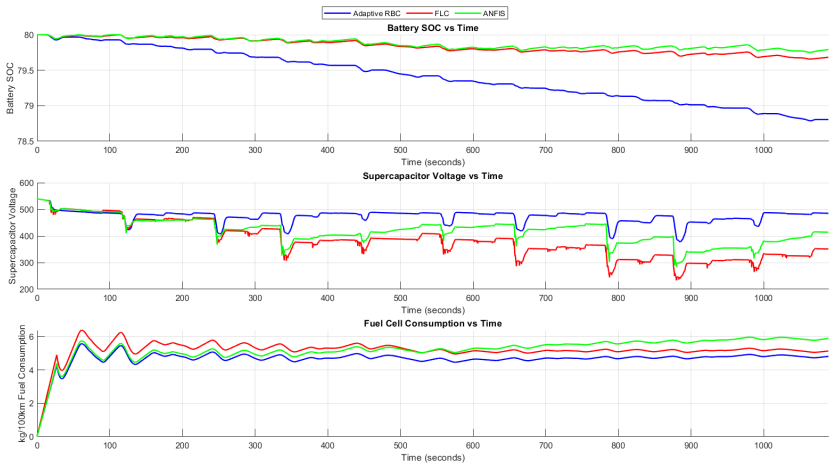

Figure 3.17: Battery SOC, Supercapacitor Voltage and FC Fuel Consumption Comparison for A-RBC, FLC, and ANFIS with Vehicle Mass = 13000kg.

As detailed in Table 3.8, the root mean square (RMS) values of the battery C-rate decreased across all scenarios, even as the number of passengers—and consequently, the vehicle mass and payload—increased. This demonstrates the superior capability

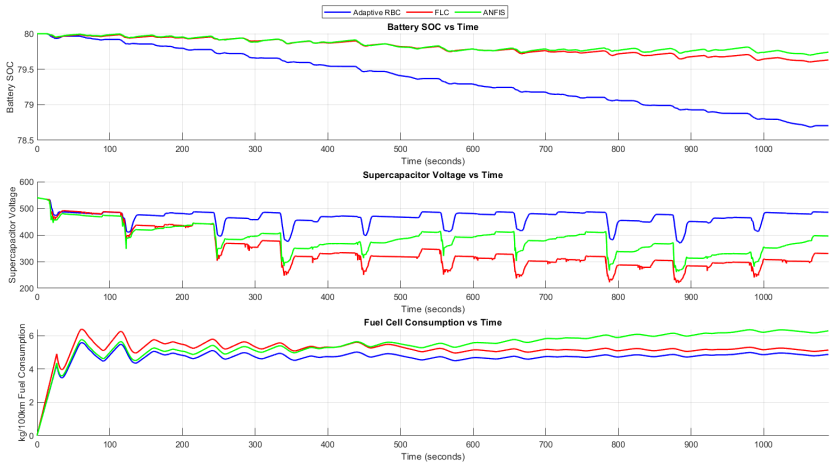

Figure 3.18: Battery SOC, Supercapacitor Voltage and FC Fuel Consumption Comparison for A-RBC, FLC, and ANFIS with Vehicle Mass = 14000kg.

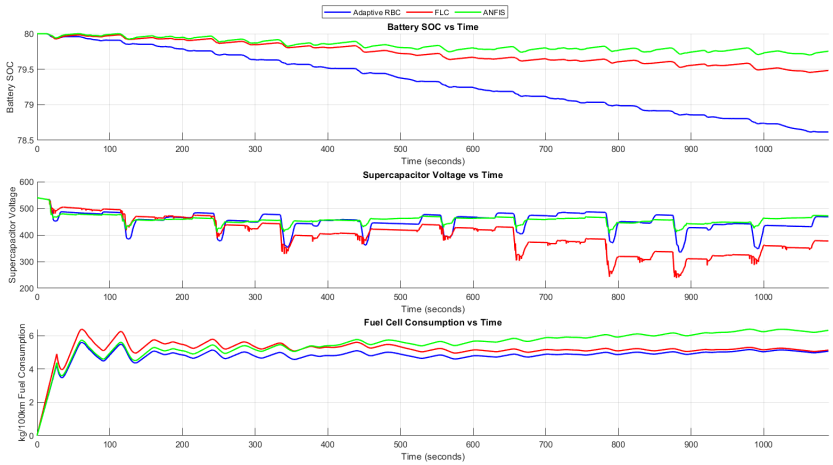

Figure 3.19: Battery SOC, Supercapacitor Voltage and FC Fuel Consumption Comparison for A-RBC, FLC, and ANFIS with Vehicle Mass = 15000kg.

of the ANFIS controller in managing energy flow between various sources, ensuring smoother battery usage. Additionally, the final state of charge at the end of the Manhattan driving cycle is higher with the ANFIS controller compared to adaptive rule-based and fuzzy logic controllers, indicating better charge-sustaining performance. The ANFIS controller effectively balances the trade-off between utilizing different energy sources to meet power demands. It is specifically tuned to minimize battery stress by leveraging the supercapacitor and fuel cell more extensively. However, maintaining the SC voltage above a critical threshold is essential to ensure it remains effective for future driving cycles and can buffer power peaks. Even with this

consideration, the ANFIS controller performed better, with the SC voltage only dropping to 75% of its nominal capacity in the worst-case scenario during the Manhattan cycle. A key trade-off involves the increased use of the FC compared to other control strategies, leading to higher fuel consumption. This can be mitigated by selecting an appropriate fuel tank size, ensuring sufficient energy buffering to support the primary objective of maintaining the battery in a charge-sustaining mode. These behaviors are illustrated in Figure 3.17, 3.18, and 3.19, highlighting the overall effectiveness of the ANFIS controller in optimizing energy management while preserving battery health and performance. In the ANFIS simulations for vehicle masses of 13,000 kg, 14,000 kg, and 15,000 kg, the RMS of battery C-rate decreased by 14%, 11.7%, and 6%, respectively, compared to the baseline controller, A-RBC as indicated in table 3.8.

Mass [kg]		**A-RBC (Baseline)**	**FLC**	**ANFIS**
13000	**RMS**	0.0937	0.0811	0.0804
	Relative Difference wrt Baseline	-	-13%	-14%
14000	**RMS**	0.094	0.087	0.083
	Relative Difference wrt Baseline	-	-7.4%	-11.7%
15000	**RMS**	0.099	0.096	0.0922
	Relative Difference wrt Baseline	-	-3%	-6%

Table 3.8: Comparison of RMS and Relative Differences for Different Masses Using A-RBC, FLC, and ANFIS.

Chapter 4

Hardware-in-the-Loop Considerations

4.1 Introduction

Hardware-in-the-Loop (HIL) testing is a vital technique for validating hybrid propulsion systems by integrating real hardware components with simulation models to create a controlled testing environment. This approach allows for a comprehensive evaluation of system performance under various conditions before actual deployment, ensuring both reliability and efficiency. HIL testing provides a critical step in bridging the gap between simulation and real-world implementation, ensuring the system performs as expected by thoroughly evaluating the interactions between physical and virtual elements of the system [36], [37].

To effectively transition from simulations to HIL testing, it is crucial to understand the considerations and preparations necessary for setting up and validating control strategies for hybrid propulsion systems. HIL testing integrates real-time simulations with physical components, enabling the evaluation of control strategies under realistic operating conditions without needing the complete system.

4.2 Overview of Hardware-in-the-Loop Test Phases

The HIL testing process involves several phases to ensure comprehensive validation and fine-tuning of hybrid propulsion systems. Initially, sensors and actuators are calibrated to guarantee accurate data acquisition and control. Baseline tests are then conducted using the simulation environment to establish performance benchmarks. Gradual integration of physical components into the simulation environment follows, allowing for the testing of their interactions with control algorithms. Performance evaluation of the integrated system is conducted under various simulated driving conditions, focusing on the efficiency and reliability of the control strategies. Based

on the test results, control algorithms and hardware configurations are refined and optimized to enhance system performance. This iterative process ensures that the hybrid propulsion system meets the desired performance criteria before deployment in real-world applications [37].

By following these steps, the transition from simulation models to a robust HIL testing environment is achieved, ultimately validating the effectiveness of the hybrid propulsion system and its control strategies. This comprehensive approach not only enhances the reliability and safety of the system but also accelerates the development process by identifying and addressing potential issues early in the design phase [36].

4.3 Test Bench Preparation for Hardware-in-the-Loop Test

The testbench setup for HIL testing replicates real-world conditions under which the hybrid propulsion system operates. Selecting appropriate hardware components is a critical preparation step for test bench setup. As mentioned before, this involves choosing sensors, actuators, and control units that can interface effectively with the simulation environment, replicating the vehicle's operational conditions to yield meaningful test results. Integrating real components, such as the modular supercapacitor bank developed during this research, is particularly significant. The modular design allows for flexible configurations, facilitating thorough testing of different control strategies under various load conditions. This step is essential for assessing the actual hardware's performance and its interaction with the control algorithms [36].

A powerful computer running real-time simulations of vehicle dynamics and control algorithms serves as the central control unit. The actual controllers and power electronics used in the vehicle are connected to this simulation environment, allowing for direct testing of control strategies. Measurement and actuation systems, including sensors and actuators, measure and apply relevant parameters like forces and torques to the physical components, ensuring accurate testing conditions. Communication interfaces such as the CAN bus facilitate seamless data exchange and control between the simulation environment and physical components [36], [37].

Moreover, setting up data acquisition systems is vital for monitoring and recording the performance of both hardware and simulation. This setup involves configuring sensors and data logging tools to capture detailed information during testing, which is crucial for analyzing and troubleshooting the system's behavior. Safety protocols are also paramount during HIL testing to handle unexpected behaviors or failures. Implementing fail-safes and emergency shutdown mechanisms ensures a safe testing environment, protecting both the equipment and operators [37].

4.4 Case Study: Test Bench Design and Setup

The HIL test bench is composed of several critical components that work together to create a realistic testing environment for hybrid electric vehicles as demonstrated in Figure 4.1. These components include electric machines, coupling mechanisms, torque meters, control units, power drivers, and a digital platform.

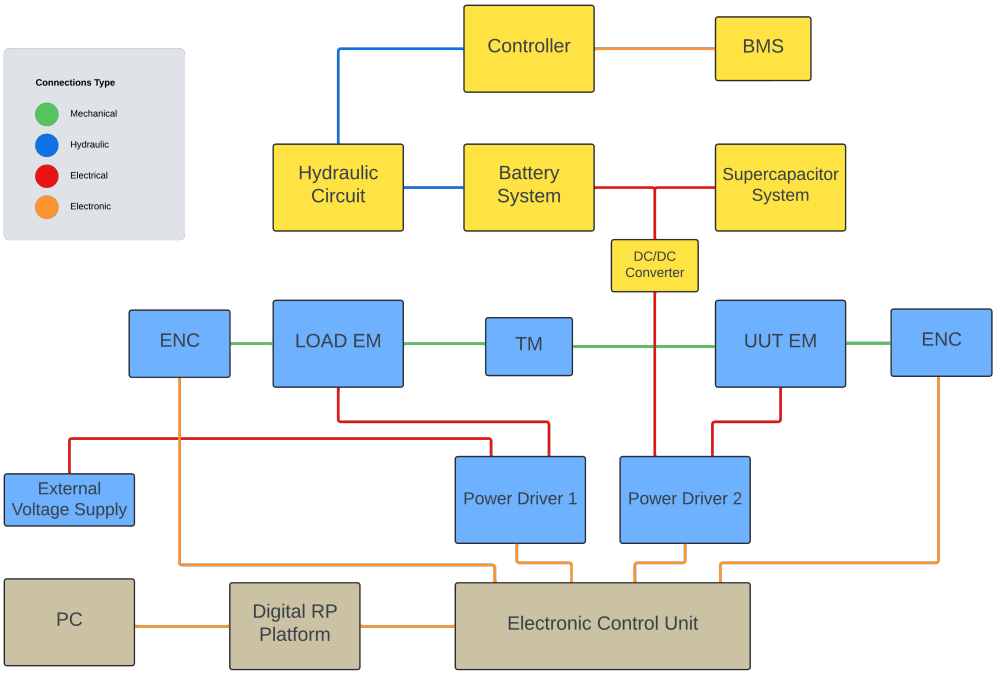

Figure 4.1: Testbench Layout Model.

The electric machines used in the test bench are Brushless DC electric motor (BLDC) motors with a power rating of 3 kW and an operating voltage of 48V. These machines simulate the traction and load motors of a vehicle, providing the mechanical load necessary to replicate various driving conditions. They are connected to the torque meter through BK2 Bellow Couplings, ensuring precise transmission of torque without any loss. They are mechanical devices used to connect two shafts together. The torque transducer, an HBM T20WN/10NM, measures the torque transmitted between the load electric machine and the unit under test (UUT) electric machine. The "10NM" indicates that this particular transducer can measure up to 10 Newton-meters of torque. It provides essential data for analyzing the system's performance and efficiency. Moreover, encoder device (ENC) is used to convert mechanical motion into electrical signals that can be read by control systems. Encoders in this setup are crucial for providing real-time feedback on the rotational position, speed, and direction of rotating components.

The control unit, a TI Launchpad F28379D, serves as the primary controller for

the test bench. This development board produced by Texas Instruments (TI), and is used to prototype and test electronic circuits and software. It manages the operation of the electric machines and ensures that the system operates according to the predefined control strategies. This unit interfaces directly with the MATLAB/Simulink environment running on the PC, enabling real-time control and adjustments based on simulation data. The power drivers, TI Launchpad Boosters (55V-30A), supply the necessary power to the electric machines, enabling them to simulate different driving conditions by ensuring the correct voltage and current supply.

The digital platform, specifically the Speedgoat target machine, acts as the real-time processing unit interfacing with MATLAB/Simulink models. It ensures that simulation data is accurately translated into real-world testing scenarios, facilitating seamless integration between the simulation environment and the physical test bench. An external voltage supply provides the necessary voltage to the test bench components, ensuring a stable power source for all systems.

The PC runs MATLAB/Simulink and other necessary software, while the digital Rapid Prototyping (RP) platform allows for rapid testing and iteration of control strategies. This setup supports the efficient development and validation of control algorithms, making the HIL test bench an essential tool for this research.

4.4.1 Integration and Workflow of Test bench

The integration of these components within the HIL test bench is designed to closely replicate real-world conditions. The control unit receives commands from the MATLAB/Simulink environment on the PC, allowing for real-time control and adjustment based on simulation data. Power drivers ensure that the electric machines receive the correct voltage and current, simulating the vehicle's traction and load conditions.

Continuous data on torque, speed, and other critical parameters is provided by the torque meter and other sensors. This data is fed back into the MATLAB/Simulink environment via the digital platform, enabling real-time analysis and adjustments. Additionally, a modular supercapacitor bank is designed and 3D printed to match the voltage and capacity requirements of the hybrid propulsion system. This modularity allows for easy reconfiguration and testing of different control strategies and load conditions. Safety features, such as overvoltage and overcurrent protection, are integrated into the design to ensure safe operation during testing.

4.4.2 Design and 3D Printing of a Modular Supercapacitor Bank

After laying the groundwork with the introduction and considerations for HIL testing, the next step is to delve into the another contributions of this thesis, particularly the design and development of a modular supercapacitor bank. This section will

focus on the design process, the steps taken to ensure modularity, and the use of 3D printing technology to realize the physical components.

To meet the voltage and capacity requirements of the hybrid propulsion system, it is crucial to determine the specifications for the supercapacitor cells. This involves calculating the number of cells needed and their configuration to achieve the desired performance. The modular design of the supercapacitor bank allows for flexible arrangements of cells to meet specific voltage and capacity needs. This modularity is essential as it provides the capability to reconfigure the cells easily, facilitating the testing of various control strategies and load conditions.

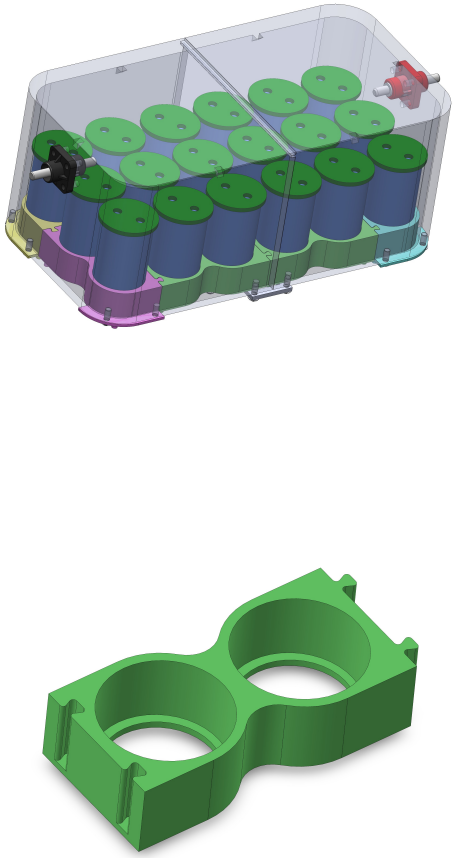

Figure 4.2: Modular Supercapacitor Bank With Circular Control Board.

Safety features are an integral part of the design. Integrating mechanisms such as control boards helps protect the system against overvoltage and overcurrent scenarios, ensuring reliable and safe operation. Moreover, quick-connect coupling connectors (RadLok) were utilized in the construction of the supercapacitor bank

because they are designed for high-current applications and provide a secure, quick-connect solution for electrical systems. They ensure low contact resistance and robust mechanical stability, which are essential for the high-power demands and frequent load changes experienced in hybrid energy storage systems. The modular SC bank's design supports the hybrid propulsion system by offering adaptable and secure energy storage solutions, enhancing the system's overall performance and testing efficiency. Based on the various types of available supercapacitor cells and their corresponding control boards, two distinct approaches were adopted to design modular holders. The first approach utilized circular control boards, connecting pairs of cells in series. These pairs could then be connected in series or parallel with other modular holders to form an SC bank with the desired voltage, as illustrated in Figure 4.2. The second approach aimed to achieve the same objective using different SC cells compatible with rectangular control boards. This involved designing holders that also allowed for series or parallel connections to reach the target voltage of the SC bank, as shown in Figure 4.3.

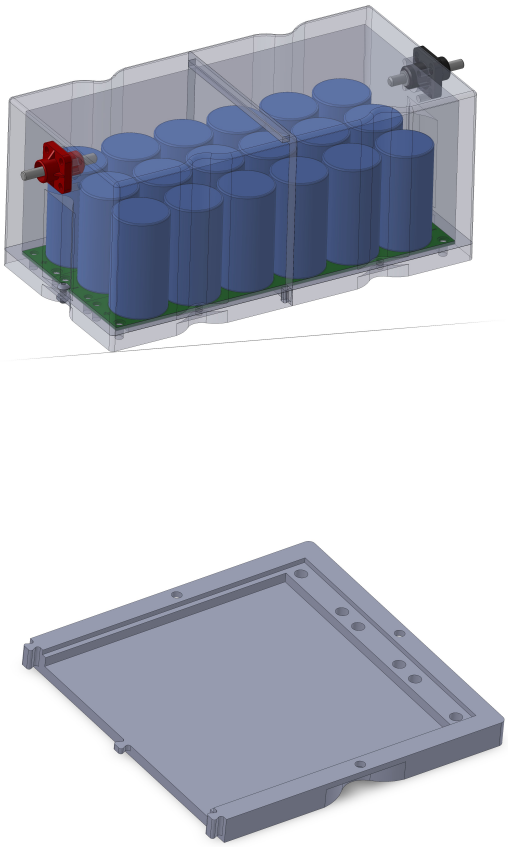

Figure 4.3: Modular Supercapacitor Bank With Triangular Control Board.

Chapter 5

Conclusion and Future Developments

The research conducted in this thesis demonstrated the significant benefits of integrating advanced energy storage systems within electric vehicles to enhance their efficiency and performance. The primary findings indicate that incorporating hybrid energy storage systems (HESS) comprising batteries, supercapacitors, and fuel cells markedly improves vehicle performance.

Initially, the integration of a supercapacitor bank alongside the battery in a Battery Electric Vehicle (BEV) significantly enhanced its ability to handle high power demands and capture regenerative braking energy. This configuration reduced battery stress and extended the battery lifespan. Further optimization was achieved by introducing a fuel cell to create a Fuel Cell Hybrid Electric Vehicle (FCHEV). This addition resulted in a reduction in the overall mass of the HESS while maintaining the vehicle's original range.

Various control strategies were explored to manage the energy distribution within these hybrid systems. Rule-based and adaptive rule-based controllers provided a baseline for energy management, with the adaptive version demonstrating improved performance by dynamically adjusting to varying driving conditions. The Fuzzy Logic Controller (FLC) effectively managed the power flow between the supercapacitor and the battery, adapting to different vehicle masses and driving cycles. Although it required careful tuning to prevent excessive supercapacitor usage, the FLC provided smooth and continuous control signals. The introduction of the Adaptive Neuro-Fuzzy Inference System (ANFIS) further enhanced the system's adaptability to changing vehicle mass and improved overall energy management. ANFIS combined the learning capabilities of neural networks with the flexibility of fuzzy logic, resulting in more efficient power distribution and improved vehicle performance under varying load conditions.

Simulations confirmed these findings, showing a 25% reduction in battery C-rate for the BEV with a supercapacitor bank and a 15% reduction in the overall mass

of the HESS for the FCHEV, while maintaining the vehicle's range. In the ANFIS simulations for vehicle masses of 13,000 kg, 14,000 kg, and 15,000 kg, the RMS of battery C-rate decreased by 14%, 11.7%, and 6%, respectively, compared to the baseline ruled-based controller.

To validate these results, Hardware-in-the-Loop (HIL) testing was proposed. This involves integrating real hardware components with simulation models to evaluate system performance under various conditions.

Future research and development should focus on enhancing control strategies, conducting long-term testing and validation, and assessing the economic and environmental impact of these systems.

Refining ANFIS and other advanced control strategies can optimize the balance between battery, supercapacitor, and fuel cell usage. Machine learning techniques can be explored to develop predictive models for energy management that adapt in real-time to changing driving conditions and vehicle states. Extended HIL testing is necessary to assess the long-term performance and durability of the proposed hybrid energy storage systems under various real-world conditions. Collaboration with industry partners for field trials will provide data on the practical implementation of these systems in commercial vehicles.

Finally, a comprehensive cost-benefit analysis of implementing these advanced hybrid systems in commercial vehicles is essential. Evaluating the environmental impact of large-scale adoption, including lifecycle assessments of the energy storage components, will ensure these advancements contribute positively to sustainable transportation solutions.

By addressing these areas, future research can significantly advance hybrid electric propulsion systems, supporting global efforts to promote sustainable transportation and enhance the operational efficiency of electric vehicles.

Bibliography

[1] *'Fit for 55': Delivering the EU's 2030 Climate Target on the Way to Climate Neutrality*. https://bit.ly/4bAcmGT. (Visited on 06/04/2024) (cit. on p. 1).

[2] Tobias Haas and Hendrik Sander. «Decarbonizing Transport in the European Union: Emission Performance Standards and the Perspectives for a European Green Deal». In: *Sustainability* 12.20 (Jan. 2020), p. 8381. ISSN: 2071-1050. DOI: 10.3390/su12208381. (Visited on 06/04/2024) (cit. on p. 1).

[3] boxcar-admin. *A World of Thoughts on Phase 2*. Sept. 2016. (Visited on 06/04/2024) (cit. on p. 1).

[4] Krishna Veer Singh, Hari Om Bansal, and Dheerendra Singh. «A Comprehensive Review on Hybrid Electric Vehicles: Architectures and Components». In: *Journal of Modern Transportation* 27.2 (June 2019), pp. 77–107. ISSN: 2196-0577. DOI: 10.1007/s40534-019-0184-3. (Visited on 06/04/2024) (cit. on p. 2).

[5] Caiying Shen, Peng Shan, and Tao Gao. «A Comprehensive Overview of Hybrid Electric Vehicles». In: *International Journal of Vehicular Technology* 2011 (Nov. 2011), e571683. ISSN: 1687-5702. DOI: 10.1155/2011/571683. (Visited on 06/04/2024) (cit. on p. 2).

[6] *WEVJ | Free Full-Text | A Comprehensive Review for Battery Electric Vehicles (BEV) Drive Circuits Technology, Operations, and Challenges*. https://www.mdpi.com/2032-6653/14/7/195. (Visited on 06/04/2024) (cit. on p. 3).

[7] *Smart Cities | Free Full-Text | A Review on Electric Vehicles: Technologies and Challenges*. (Visited on 06/04/2024) (cit. on p. 3).

[8] Sivapriya Mothilal Bhagavathy, Hannah Budnitz, Tim Schwanen, and Malcolm McCulloch. «Impact of Charging Rates on Electric Vehicle Battery Life». In: *Findings* (Mar. 2021). DOI: 10.32866/001c.21459. (Visited on 06/04/2024) (cit. on p. 4).

[9] *Automotive Electricity: Electric Drives | Wiley*. https://www.wiley.com/en-sg/Automotive+Electricity%3A+Electric+Drives-p-9781118617373. (Visited on 06/10/2024) (cit. on p. 4).

[10] Ahmed Ragab, Mostafa I. Marei, and Mohamed Mokhtar. «Comprehensive Study of Fuel Cell Hybrid Electric Vehicles: Classification, Topologies, and Control System Comparisons». In: *Applied Sciences* 13.24 (Jan. 2023), p. 13057. ISSN: 2076-3417. DOI: 10.3390/app132413057. (Visited on 06/04/2024) (cit. on p. 4).

[11] Antonio García, Javier Monsalve-Serrano, Rafael Lago Sari, and Shashwat Tripathi. «Life Cycle CO_2 Footprint Reduction Comparison of Hybrid and Electric Buses for Bus Transit Networks». In: *Applied Energy* 308 (Feb. 2022), p. 118354. ISSN: 0306-2619. DOI: 10.1016/j.apenergy.2021.118354. (Visited on 06/04/2024) (cit. on p. 5).

[12] Pengli Yu, Mince Li, Yujie Wang, and Zonghai Chen. «Fuel Cell Hybrid Electric Vehicles: A Review of Topologies and Energy Management Strategies». In: *World Electric Vehicle Journal* 13.9 (Sept. 2022), p. 172. ISSN: 2032-6653. DOI: 10.3390/wevj13090172. (Visited on 06/04/2024) (cit. on p. 5).

[13] Mustafa Ergin Şahin, Frede Blaabjerg, and Ariya Sangwongwanich. «A Comprehensive Review on Supercapacitor Applications and Developments». In: *Energies* 15.3 (Jan. 2022), p. 674. ISSN: 1996-1073. DOI: 10.3390/en15030674. (Visited on 06/04/2024) (cit. on pp. 5, 6).

[14] *Forecasting | Free Full-Text | Comprehensive Review of Power Electronic Converters in Electric Vehicle Applications*. https://www.mdpi.com/2571-9394/5/1/2 (Visited on 06/04/2024) (cit. on p. 6).

[15] *The Structure and Control Method of Hybrid Power Source for Electric Vehicle - ScienceDirect*. https://bit.ly/3XXj4Dz. (Visited on 06/04/2024) (cit. on pp. 6, 20).

[16] Lia Kouchachvili, Wahiba Yaïci, and Evgueniy Entchev. «Hybrid Battery/-Supercapacitor Energy Storage System for the Electric Vehicles». In: *Journal of Power Sources* 374 (Jan. 2018), pp. 237–248. ISSN: 0378-7753. DOI: 10.1016/j.jpowsour.2017.11.040. (Visited on 06/04/2024) (cit. on p. 7).

[17] Changle Xiang, Yanzi Wang, Sideng Hu, and Weida Wang. «A New Topology and Control Strategy for a Hybrid Battery-Ultracapacitor Energy Storage System». In: *Energies* 7.5 (May 2014), pp. 2874–2896. ISSN: 1996-1073. DOI: 10.3390/en7052874. (Visited on 06/04/2024) (cit. on p. 7).

[18] Dawei Gao, Zhenhua Jin, and Qingchun Lu. «Energy Management Strategy Based on Fuzzy Logic for a Fuel Cell Hybrid Bus». In: *Journal of Power Sources* 185.1 (Oct. 2008), pp. 311–317. ISSN: 0378-7753. DOI: 10.1016/j.jpowsour.2008.06.083. (Visited on 06/04/2024) (cit. on pp. 8, 44).

[19] Yuzheng Zhu, Xueyuan Li, Qi Liu, Songhao Li, and Yao Xu. «Review Article: A Comprehensive Review of Energy Management Strategies for Hybrid Electric Vehicles». In: *Mechanical Sciences* 13.1 (Mar. 2022), pp. 147–188. ISSN: 2191-9151. DOI: 10.5194/ms-13-147-2022. (Visited on 06/04/2024) (cit. on pp. 8, 11).

[20] Ouafae El Ganaoui-Mourlan et al. «Design of a Flexible Hybrid Powertrain Using a 48 V-Battery and a Supercapacitor for Ultra-Light Urban Vehicles». In: *WCX SAE World Congress Experience*. SAE International, Apr. 2020. DOI: 10.4271/2020-01-0445. (Visited on 06/04/2024) (cit. on p. 9).

[21] Siang Fui Tie and Chee Wei Tan. «A Review of Energy Sources and Energy Management System in Electric Vehicles». In: *Renewable and Sustainable Energy Reviews* 20 (Apr. 2013), pp. 82–102. ISSN: 1364-0321. DOI: 10.1016/j.rser.2012.11.077. (Visited on 06/06/2024) (cit. on p. 9).

[22] *Applied Sciences / Free Full-Text / Fuzzy Logic-Based Duty Cycle Controller for the Energy Management System of Hybrid Electric Vehicles with Hybrid Energy Storage System*. https://www.mdpi.com/2076-3417/11/7/3192. (Visited on 06/10/2024) (cit. on pp. 10, 11).

[23] E.H. Mamdani and S. Assilian. «An Experiment in Linguistic Synthesis with a Fuzzy Logic Controller». In: *International Journal of Man-Machine Studies* 7.1 (Jan. 1975), pp. 1–13. ISSN: 00207373. DOI: 10.1016/S0020-7373(75)80002-2. (Visited on 06/10/2024) (cit. on p. 11).

[24] Navneet Walia, Harsukhpreet Singh, and Anurag Sharma. «ANFIS: Adaptive Neuro-Fuzzy Inference System- A Survey». In: *International Journal of Computer Applications* 123.13 (Aug. 2015), pp. 32–38. (Visited on 06/13/2024) (cit. on p. 11).

[25] Chan-Uk Yeom and Keun-Chang Kwak. «Adaptive Neuro-Fuzzy Inference System Predictor with an Incremental Tree Structure Based on a Context-Based Fuzzy Clustering Approach». In: *Applied Sciences* 10.23 (Jan. 2020), p. 8495. ISSN: 2076-3417. DOI: 10.3390/app10238495. (Visited on 06/13/2024) (cit. on p. 11).

[26] Jiankun Peng, Jiwan Jiang, Fan Ding, and Huachun Tan. «Development of Driving Cycle Construction for Hybrid Electric Bus: A Case Study in Zhengzhou, China». In: *Sustainability* 12.17 (Jan. 2020), p. 7188. ISSN: 2071-1050. DOI: 10.3390/su12177188. (Visited on 06/07/2024) (cit. on p. 16).

[27] Souleman Njoya Motapon, Louis-A. Dessaint, and Kamal Al-Haddad. «A Comparative Study of Energy Management Schemes for a Fuel-Cell Hybrid Emergency Power System of More-Electric Aircraft». In: *IEEE Transactions on Industrial Electronics* 61.3 (Mar. 2014), pp. 1320–1334. ISSN: 1557-9948. DOI: 10.1109/TIE.2013.2257152. (Visited on 06/08/2024) (cit. on p. 23).

[28] L. Zubieta and R. Bonert. «Characterization of Double-Layer Capacitors for Power Electronics Applications». In: *IEEE Transactions on Industry Applications* 36.1 (Jan. 2000), pp. 199–205. ISSN: 1939-9367. DOI: 10.1109/28.821816. (Visited on 06/08/2024) (cit. on p. 23).

[29] C. H. Wu, Y. H. Hung, and C. W. Hong. «On-Line Supercapacitor Dynamic Models for Energy Conversion and Management». In: *Energy Conversion and Management* 53.1 (Jan. 2012), pp. 337–345. ISSN: 0196-8904. DOI: 10.1016/j.enconman.2011.01.018. (Visited on 06/08/2024) (cit. on p. 23).

[30] object Object. «Modeling and Model Validation of Supercapacitors for Real-Time Simulations». In: (). (Visited on 06/08/2024) (cit. on p. 23).

[31] A. Foelske, O. Barbieri, M. Hahn, and R. Kötz. «An X-Ray Photoelectron Spectroscopy Study of Hydrous Ruthenium Oxide Powders with Various Water Contents for Supercapacitors». In: *Electrochemical and Solid-State Letters* 9.6 (Apr. 2006), A268. ISSN: 1944-8775. DOI: 10.1149/1.2188078. (Visited on 06/08/2024) (cit. on p. 26).

[32] FuelCellsWorks. *Horizon Automotive PEM Fuel Cells To Set 300kW Benchmark - FuelCellsWorks*. (Visited on 06/10/2024) (cit. on p. 45).

[33] Jennifer Bauman and Mehrdad Kazerani. «A Comparative Study of Fuel-Cell–Battery, Fuel-Cell–Ultracapacitor, and Fuel-Cell–Battery–Ultracapacitor Vehicles». In: *IEEE Transactions on Vehicular Technology* 57.2 (Mar. 2008), pp. 760–769. ISSN: 1939-9359. DOI: 10.1109/TVT.2007.906379. (Visited on 06/10/2024) (cit. on p. 45).

[34] Souleman Njoya M., Olivier Tremblay, and Louis-A. Dessaint. «A Generic Fuel Cell Model for the Simulation of Fuel Cell Vehicles». In: *2009 IEEE Vehicle Power and Propulsion Conference*. Sept. 2009, pp. 1722–1729. DOI: 10.1109/VPPC.2009.5289692. (Visited on 06/10/2024) (cit. on p. 46).

[35] D. Wilson, A. Bousbaine, and J. Andrade. «Simulink Model for a Hydrogen PEM Fuel Cell for Automotive Applications». In: *The 10th International Conference on Power Electronics, Machines and Drives (PEMD 2020)*. Vol. 2020. Dec. 2020, pp. 146–151. DOI: 10.1049/icp.2021.1176. (Visited on 06/10/2024) (cit. on p. 47).

[36] Valerio Martini, Francesco Mocera, and Aurelio Somà. «Design and Experimental Validation of a Scaled Test Bench for the Emulation of a Hybrid Fuel Cell Powertrain for Agricultural Tractors». In: *Applied Sciences* 13.15 (Jan. 2023), p. 8582. ISSN: 2076-3417. DOI: 10.3390/app13158582. (Visited on 06/13/2024) (cit. on pp. 47, 65, 66).

[37] Manfredi Tornabene, Gennaro Sorrentino, Renato Galluzzi, Andrea Tonoli, and Nicola Amati. «A Hardware-in-the-Loop Approach to Test Rotary Electromagnetic Shock Absorbers». In: *IEEE Access* 12 (2024), pp. 67486–67497. ISSN: 2169-3536. DOI: 10.1109/ACCESS.2024.3400676. (Visited on 06/13/2024) (cit. on pp. 65, 66).